Climate Dynamics
https://doi.org/10.1007/s00382-020-05387-z

Role of convective and microphysical processes on the simulation of monsoon intraseasonal oscillation

Ushnanshu Dutta[1,2] · Hemantkumar S. Chaudhari[1] · Anupam Hazra[1] · Samir Pokhrel[1] · Subodh Kumar Saha[1] · Chinta Veeranjaneyulu[1]

Received: 24 July 2019 / Accepted: 21 July 2020

Abstract

The study explores the role of ice-phase microphysics and convection for the better simulation of Indian summer monsoon rainfall (ISMR) and monsoon intraseasonal oscillation (MISO). Sensitivity experiments have been performed with coupled climate model- CFSv2 using different microphysics (with and without ice phase processes) and convective [Simple Arakawa Schubert (SAS), new SAS (NSAS)] parameterization schemes. Results reveal that the ice phase microphysics parameterization scheme performs better in the simulation of active and break composites of the ISMR as compared to ice-free runs. The difference between ice (ICE) and ice-free run (NOICE) can be attributed to the availability of copious cloud condensate at the upper level. Better representation of upper-level cloud condensate in ICE run (i.e., with ice phase microphysics) leads to correct representation of specific humidity in active and break spells. Proper depiction of upper-level cloud condensate further leads to realistic modulation of atmospheric circulation and better simulation of convection (as represented by OLR) in active and break spells of ICE run. As a result, better simulation of active and break occurs in the ICE run. In contrast, NOICE run (i.e., with warm phase microphysics) fails to depict upper-level cloud condensate in the active phase. It leads to an improper representation of specific humidity. Circulation features are also unrealistic, and convection is suppressed in the active phase. As a result, the active phase is not adequately simulated in the NOICE run. NOICE run composites during active spells depict the overestimation of the ascending branch of Hadley circulation as compared to MERRA reanalysis, which is relatively better in ICE run. NOICE run composites during active spells depict the overestimation of the ascending branch of Walker circulation as compared to MERRA reanalysis, which is further improved in ICE runs. The north–south space–time spectra of daily rainfall anomaly are also better captured by ICE run as compared to NOICE run. Results indicate that ice-phase processes are more important for capturing the difference between active and break composites, while convection parameterization is relatively more important for the intraseasonal variance analyses. Further improvements in ice microphysics parameterization with better convection schemes in models will be helpful for the betterment of MISO and will lead to the improved simulation of monsoon.

1 Introduction

The interannual variability (IAV) of the Indian Summer Monsoon (ISM) rainfall (ISMR) has a significant impact on the socio-economic conditions of the people in this region (Parthasarathy et al. 1988; Gadgil 2007). The Indian summer monsoon is a coupled climate system (Webster et al. 1998). Therefore, the coupled global land–atmosphere-ocean model is essential for the simulation of the ISM climate (Wang 2005; Chaudhari et al. 2013) on the sub-seasonal (i.e., active-break cycles) to seasonal time scales. The seasonal mean monsoon rainfall is the sum of contributions from vigorous sub-seasonal oscillations (i.e., active and break spells) and synoptic disturbances that form within the sub-seasonal

Electronic supplementary material The online version of this article (https://doi.org/10.1007/s00382-020-05387-z) contains supplementary material, which is available to authorized users.

✉ Hemantkumar S. Chaudhari
hemantkumar@tropmet.res.in

[1] Indian Institute of Tropical Meteorology, Dr.Homi Bhabha Road, NCL Post, Pashan, Pune 411008, India

[2] Department of Atmospheric and Space Sciences, Savitribai Phule Pune University, Pune, India

Published online: 01 August 2020

spells (Saha et al. 2019). In the temporal domain, the monsoon intraseasonal oscillations (MISOs) are dominated by 30–60 days and 10–20 days modes. The northward propagation of 30–60 days mode and westward propagation of 10–20 days mode are essential characteristics of ISMR. Several studies have pointed out that improvements in the skill of ISMR by coupled global climate models (CGCMs) are very marginal, and the skill score remains significantly below the potential limit of predictability (e.g., Krishna Kumar et al. 2005; Rajeevan et al. 2012). However, a recent study (Saha et al. 2019) has pointed out that higher ISMR skills in the coupled model can be achieved by improving ISM subseasonal fluctuations through improvements in model physics.

There are several complex multi-scale processes, which includes the large-scale moisture convergence as well as microphysical processes of raindrop formation (e.g., autoconversion, rain accretion, snow accretion, and melting) (Zhao and Carr 1997; Sundqvist et al. 1989; Tao and Moncrieff 2009; Hazra et al. 2015, 2016), govern the total rainfall. Hence, lack of knowledge of cloud processes and precipitation physics on the MISO scale is one of the major deficiencies in simulating the observed MISOs by the climate models (Kumar et al. 2017; Hazra et al. 2017a, b). Hong et al. (2004) found that modifications in the ice microphysical processes may result in a more realistic distribution of clouds. Stratiform rain is very much associated with the formation of cloud condensate, particularly the cloud ice and mixed-phase hydrometeors (Liu et al. 2007; Fu et al. 2011; Kumar et al. 2014; Field and Heymsfield 2015). Therefore stratiform rain has a large impact on ISMR (e.g., Rajeevan et al. 2012). It has been discovered that the stratiform rain fraction plays a critical role in the organization of clouds and precipitation in MISOs through modification of the vertical profile of heating, which results in large-scale low-level moisture convergence (e.g., Kumar et al. 2017). Satellite observations over the Indian summer monsoon region also indicate that about 40–50% of rainfall events originate from the melting of ice (Field and Heymsfield 2015), which confirms the more significant role of ice processes. Earlier studies have demonstrated that cirrus clouds comprised of ice crystals have an annual global average frequency of occurrence of about 30% (Wylie and Menzel 1999; Wang et al. 1996; Rossow and Schiffer 1999).

Historically saying, the importance of ice-microphysics to precipitation is known to the scientific community for long years starting from the theory of Bergeron (1935), who emphasized the importance of lower vapor pressure over ice in an environment in which ice crystals and water-droplets coexist. Earlier, McCumber et al. (1991) have shown that convection simulation gets improved with the increase in the number of ice-categories. They also found that anvil heating in the middle and upper troposphere was also more for ice-case than that of the ice-free case, which had significantly influenced the simulation of cloud processes. Boyle et al. (2015) carried out an extensive analysis of the sensitivity of Madden–Julian oscillation to different model physical parameters. Yang et al. (2015) studied the sensitivity of Asian summer monsoon to physical processes related to microphysics and convection. The deep convective cloud contains a considerable amount of ice as well as other frozen hydrometeors (Kruegera et al. 1995; Rossow and Schiffer 1999). Based on ten years of the climatology of total cloud fraction data of Cloud-Aerosol Lidar and Infrared Pathfinder Satellite Observation (CALIPSO) during June–September (JJAS; Supplementary Fig. 1a–i) in the Extended Indian Summer Monsoon Region (40° E–120° E, 30° S–30° N), it is also found that Ice Cloud Fraction (ICF) is dominant in the high level (altitude > 6.5 km) clouds (Supplementary Fig. 1f), whereas liquid cloud fraction (LCF) is dominant in the mid-level (3.2 km < altitude < 6.5 km) and the low-level clouds (altitude < 3.2 km). There is a considerable amount of LCF available in the mid-level clouds, and a moderate amount of LCF at high-level clouds is also seen (Supplementary Fig. 1k, j). This might be attributed to the mixed-phase in high-level clouds and the melting of ice in mid-level clouds.

The cloud microphysical processes, in general, influence the large-scale circulation (Bony et al. 2015; De et al. 2016, 2019; Chaudhari et al. 2018) in two aspects: (a) total heating and (b) heating profile. The total heating is composed of latent heating, radiative (shortwave and longwave) heating, and sensible heating, where latent heating is considered as the most dominant part (Hazra et al. 2017a). The effect of ice microphysics in the global coupled model also significantly alters the radiation feedbacks. Excessive longwave radiation heating, due to trapping by too much ice cloud present above, may lead to warm-bias whereas a diminution of shortwave heating in the troposphere due to cirrus-shading will lead a reverse effect to that of the longwave (Hong et al. 2004). Choudhury and Krishnan (2011) have shown that improvement in the vertical profile of heating, as a result of the increased contribution of stratiform rain fraction, leads to improvement in northward propagation of the MISO.

Hazra et al. (2017b) introduced a physically-based modification of Zhao and Carr (1997) cloud microphysics scheme in CFSv2 (NCEP coupled climate model) along with the modified new simple Arakawa-Schubert convective parameterization of Han and Pan (2011). These improvements indicate that the model can capture the observed space–time spectra and amplitude of MISO. Ice processes play a key role in shaping the rainfall amount, intensity, and distribution over the Indian summer monsoon region. In another study, Abhik et al. (2017) have introduced the six-class WRF single moment (WSM6) microphysical scheme in CFSv2 by replacing the existing simple cloud microphysics along

with new SAS cumulus scheme for the improved mean and intraseasonal variability of ISM. Recently, the stochastic representation of organized convection in CFSv2 has been reported to improve the synoptic and intraseasonal variability of the ISM (e.g., Goswami et al. 2017). Heated condensation framework has been demonstrated as a convective triggering criterion into the CFSv2 model for the improvement of the Indian summer monsoon (e.g., Bombardi et al. 2015). Incorporation of microphysical processes into CGCMs may lead to augment the understanding of MISOs (e.g., Zhang and Song 2016). The identification of cloud processes in the ISM region and the use of proper convective microphysics parameterization in CFSv2 may lead to an improvement in ISM representation. Rajeevan et al. (2012) using Cloudsat data and Abhik et al. (2014) using TRMM data have demonstrated that the proper vertical distribution of cloud is important for intraseasonal oscillations (ISO). So, there is a need for proper representation of thermodynamics (heating and cooling distribution) and dynamics in coupled climate models to address the concern. Thus, better convective microphysics parameterization for the coupled models is essential.

Sensitivity of different convective parameterization schemes for the simulation of Indian Summer Monsoon using the regional and global model have been explored by several researchers. Kang and Hong (2008) compared four different convective parameterized schemes (the Simplified ArakawaSchubert (SAS), Relaxed Arakawa Schubert (RAS), NCAR Community Climate Model version 3 (CCM), and Kain Fritsch (KF2)) in National Centers for the Environmental Prediction regional spectral model to study their impact on East Asian summer monsoon climatology. Mukhopadhyay et al. (2010) also compared three convective parameterization schemes, namely the Grell–Devenyi (GD), the Betts–Miller–Janjić (BMJ), and the Kain–Fritsch (KF) in Weather Research Forecast (WRF) model. Chakraborty and Nanjundiah (2014) compared SAS and Kuo Cumulus Parameterization (Anthes 1977) schemes from the perspective of the role of orography in convection. Pattanaik et al. (2013) compared SAS and Relaxed SAS (RAS) in which they found that SAS has more skill in extended range forecast of rainfall over Indian landmass than RAS. The new SAS (NSAS; Han and Pan 2011) convective parameterization scheme was expected to make cumulus convection stronger and deeper and enhances instability in the atmospheric column in the atmospheric component of the CFS model (the GFS model). Ganai et al. (2015) and Krishna et al. (2019) have made the comparison of convective parameterizations of SAS and revised SAS (NSAS in this study) for ISMR in seasonal scale. The use of NSAS in CFSv2 resulted in an improved simulation of the diurnal cycle of rainfall and some reduction in the dry bias over the continent (e.g., Ganai et al. 2015); but, dry (wet) rainfall bias persists over land (ocean). However, the effect of different convective parameterizations in MISO are discussed in limited studies (e.g., Ham and Hong 2013; Umakanth et al. 2015; Ganai et al. 2016). On the other hand, the sensitivity of different microphysical parameterization schemes for the simulation of ISM was explored in a handful of studies (Chaudhari et al. 2016a, b; Hazra et al. 2015, 2017a) using the global model. These studies were also limited to seasonal scale. For example, Hazra et al. (2017a) have studied the role of ice-phase microphysics on ISMR in seasonal scale using the CFSv2 model. Few studies have shown the effect of ice-free (warm) and ice-cloud (cold) microphysics in the Weather-Research forecasting (WRF) model (Fu et al. 2011) and global nonhydrostatic model without cumulus parameterization (Noda et al. 2015). However, these studies (e.g., Fu et al. 2011) were limited to the regional model. Due to a lack of such studies (e.g., Hazra et al., 2017a) based on fully coupled atmosphere–ocean models, the detailed understanding of the microphysical processes inside the convective parameterization (Zhang and Song 2016; Sud and Walker 1999) is limited. Liu et al. (2018) also highlighted that most convective parameterization schemes consider 'simple physical assumption' for the formation of rain and snow instead of the detailed microphysical process behind. Song and Zhang (2011) also suggested that the microphysical parameterization scheme must be incorporated with the convective parameterization scheme to simulate the convective to stratiform rain ratio realistically. Yang et al. (2015) also mentioned the need for comparative studies based on different cloud and convection parameterization schemes to reduce the model biases.

The detailed understanding of the impact of different microphysical parameterization schemes (warm and mixed-phase microphysics) in conjunction with different convective parameterization schemes (SAS and NSAS) for Indian summer monsoon rainfall on intraseasonal scales using CFSv2 is not reported so far. Therefore, we target to find a better convective microphysical parameterization scheme, which can be useful to simulate the active-break phases as well as intraseasonal variability of the ISM with considerable fidelity. The study aims to address the following three questions-

- Is a warm microphysics scheme (Sundqvist et al. 1989) sufficient to depict the features of active-break phases of monsoon and MISO?
- What is the role of mixed-phase microphysics (i.e., combination of ice-phase microphysics (Zhao and Carr 1997) and warm phase microphysics (Sundqvist et al. 1989) for the active-break and MISO simulation?
- Which combination of convective parameterization scheme (NSAS and SAS) with two different types of microphysics (warm and mixed-phase microphysics) will lead to better simulation of active-break and MISO?

The study is organized as follows: Sect. 2 deals with the model description and design of numerical experiments. Section 3 introduces the data used in the study. Section 4 illustrates large scale features along with MISO structures for different sensitivity experiments. Conclusions are stated in Sect. 5.

2 Model description and design of model experiments

2.1 Model description

The coupled climate model from the National Centers for Environmental Prediction (NCEP) Climate Forecast System version 2 (CFSv2) is used in the present study, which is also nowadays used for sub-seasonal to seasonal forecasting at numerous forecast centers. NCEP has developed this fully coupled ocean–atmosphere-land model, including several physical parameters with enhanced resolution and advanced initialization (Saha et al. 2014a). CFSv2 is comprised of a spectral atmospheric model, which has a resolution of T126 (~ 0.937°) with 64 hybrid vertical levels and the Geophysical Fluid Dynamics Laboratory (GFDL) Modular Ocean Model, version 4p0d (Griffies et al. 2005) at 0.25°–0.5° grid spacing with 40 vertical layers. It implements the orographic gravity wave drag and sub-grid scale mountain blocking based on Kim and Arakawa (1995) approach and Lott and Miller (1997), respectively. The four-layer Noah land surface model is coupled to CFSv2 (Ek et al. 2003). The CFSv2 model uses the Rapid Radiative Transfer Model (RRTM) shortwave radiation with maximum random cloud overlap (Mlawer et al. 1997; Iacono et al. 2000; Clough et al. 2005). The advanced cloud–radiation interaction scheme in CFSv2 can deal with the unresolved variability of layered cloud (Saha et al. 2014a). Two convective parameterization schemes (Simple Arakawa Schubert (SAS), Arakawa and Schubert 1974; and new SAS (NSAS), Han and Pan 2011) are used in this study. Cloud microphysics schemes within the CFSv2 model are Zhao and Carr (1997) and Bred Ferrier (Ferrier et al. 2002). Chaudhari et al. (2016a) have pointed out that ZC (Zhao and Carr 1997) microphysics scheme of CFSv2 is relatively better as compared to Bred-Ferrier microphysics scheme. Therefore in the current study, we have focused on the ZC microphysics scheme.

In Zhao and Carr (1997) cloud microphysics scheme, the formation of clouds from water vapor is occurred by via two condensation processes i.e., (1) large scale condensation (Sundqvist 1988) and (2) convective condensation (Betts and Miller 1986). Then, the partitioning of cloud hydrometeors and ice hydrometeors, which is based on temperature, has been done in convective schemes (SAS or NSAS) and followed by a microphysics scheme. The formation of mixed-phase hydrometeors (i.e., snow) from ice occurrs through autoconversion of snow (i.e., ice to snow autoconversion) and aggregation (i.e., collection of ice to form snow) in the microphysical scheme (as discussed in Zhao and Carr 1997). The formation of rain occurs from the warm cloud (i.e., through rain autoconversion of cloud to rain) and cold cloud (i.e., melting of snow to rain) processes, which is collectively called as mixed-phase (warm + cold) microphysical process. The warm phase microphysical process (i.e., autoconversion of rain) is guided by Sundqvist et al. (1989) scheme.

2.2 Design of model experiments

In this study, convective parameterization schemes (SAS or NSAS) controls cloud formation from water vapor and partitioning of cloud water and cloud ice (based on temperature). The formation of convective rain from cloud is based on convective autoconversion, where autoconversion function by Lord (1982) is used. For ICE-run in conjunction with two convective schemes (NSAS-ICE and SAS-ICE), the stratiform rain formation is guided by a mixed-phase (warm + cold) microphysical process (Zhao and Carr 1997). NOICE-run in conjunction with two convective schemes (NSAS-NOICE and SAS-NOICE) is guided by solely warm phase microphysical process (Sundqvist et al. 1989).

Thus, four experiments are labeled as:

(1) NSAS convection with no ICE/warm microphysics (NSAS-NOICE), (2) SAS convection with no ICE/warm microphysics (SAS-NOICE), (3) new SAS convection with ICE/mix-phase microphysics (NSAS-ICE) and (4) SAS convection with ICE/mix-phase microphysics(SAS-ICE).

The role of convective parameterization (i.e., SAS and NSAS) in association with warm and cold microphysics (NOICE and ICE) is also investigated. In each set of experiments, the CFSv2 model has been initialized by the same initial conditions, and the model is integrated for 15 years. The last 10 years of the model run are considered for the analysis, and the first 5 years are taken out for the spin-up purpose. Model initialization was done by the atmospheric and oceanic initial conditions based on climate forecast system reanalysis (CFSR). The simplified schematic of the model experiments is shown in Supplementary Fig. 7.

3 Other datasets used and methodology adopted

3.1 Other datasets used

Observed rainfall data sets are based on the Global Precipitation Climatology Project (GPCP) (Adler et al. 2003) during the period 1999–2008. The cloud fraction data are

from the Cloud-Aerosol Lidar and Infrared Pathfinder Satellite Observation (CALIPSO; Hu et al. 2009). The National Oceanic and Atmospheric Administration (NOAA) outgoing longwave radiation (OLR) data (Liebmann and Smith 1996) is also used for the analysis. Wind, cloud condensate, and specific humidity datasets are taken from Modern-Era Retrospective analysis for Research and Applications (MERRA) (Rienecker et al. 2011) for the same period.

3.2 Methodology adopted

Active and break events were calculated from the standardized time series of daily rainfall. For the same, average daily rainfall anomaly over the central Indian core monsoon region (i.e., averaged over 74° E–86° E and 16° N–26° N) is divided by the standard deviation. The selection of the region is mostly consistent with the earlier studies (e.g., Krishnamurti and Bhalme 1976, Mandke et al. 2007). The active and break spells are considered as the periods during which the standardized daily rainfall (unfiltered) anomaly is more than + 1.0 and less than − 1.0, respectively, for consecutively three days or more (Rajeevan et al. 2010). Intraseasonal oscillations (ISOs) in different bands were calculated by applying the Lanczos band-pass filter (20–100 days, 10–20 days, and 30–60 days) for daily rainfall anomaly.

4 Background large scale features during active and break spells of monsoon

The frequency of active and break spells regulates the seasonal mean rainfall, and it is of great importance for agricultural production. There are many studies available on active and break periods by mainly the use of rainfall datasets (Krishnamurti and Bhalme 1976; Mandke et al. 2007; Rajeevan et al. 2010; Abhilash et al. 2014). However, limited studies (Fu et al. 2011; Hazra et al. 2017a; Noda et al. 2015) have investigated the significance of ice-phase microphysics in monsoon convective systems. Earlier studies (Annamali and Slingo 2001) have shown that large scale flows and tropospheric circulations play an essential role in the Active-Break phase as well as MISO. However, the role of the ice-phase microphysics in the active-break phase, 10–20 day (Quasi bi-weekly mode), and 30–60 day (ISO) mode remained unexplored. Hence, the possible role of ice-phase microphysics on monsoon circulation needs to be investigated along with rainfall and OLR distribution.

4.1 Rainfall distribution and large scale convection

The spatial pattern of rainfall composites for active, break, and their difference (i.e., active minus break) is presented in Fig. 1a–o for observation (GPCP) and four sets of model experiments (i.e., NSAS-NOICE, NSAS-ICE, SAS-NOICE, and SAS-ICE). The underestimation of positive rainfall anomaly over the Indian land region and adjoining Bay of Bengal (BoB) region during active spell composites is evident, especially during NOICE runs (i.e., NSAS-NOICE, SAS-NOICE; Fig. 1b, d) as compared to observation (Fig. 1a). These findings are consistent with the study performed by Hazra et al. (2017a), where they emphasized that ICE-run leads to higher ISMR as compared to NOICE run. In the case of NSAS-ICE, active spells composites also show an underestimation of positive rainfall anomaly over the Indian region (Fig. 1c). However, oceanic features are better captured in the NSAS-ICE run as compared to NOICE runs (Fig. 1b, d). SAS-ICE depicts relatively better patterns over Indian landmass during active spells (Fig. 1e). However, over the western tropical Indian oceanic region, the extension of positive rainfall anomaly is marginally underestimated as compared to the observation.

In break composites, NOICE experiments NSAS-NOICE, SAS-NOICE show underestimation of negative rainfall anomalies over the Indian land region (Fig. 1g, i). NSAS-NOICE (Fig. 1g) simulates a more positive rainfall anomaly near the Western Ghats region. SAS-ICE and NSAS-ICE also show an underestimation of negative rainfall anomalies over India (Fig. 1j, h). However, SAS-ICE break composite anomaly patterns are relatively better as compared to other sensitivity experiments (Fig. 1j). It is evident in differences between active and break spells composites (Fig. 1k–o) that SAS-ICE is more realistic in the simulation of rainfall distribution during active and break phases. This signifies the importance of ice processes in the depiction of the correct pattern of rainfall anomaly. Warm microphysics, along with convection, leads to an underestimation of rainfall over the Indian land region. Mixed-phase microphysics, along with SAS, provides relatively better results. The difference might be due to the presence of cloud condensate at the upper level in case of ICE run, which is not happening in NOICE run (discussed in Sect. 4.3). As a result, NOICE run has limited success in the representation of large-scale monsoon circulation due to weak upper-level heating (e.g., Hazra et al. 2017a, b). For quantitative analysis (Table 1), we have computed active and break ISMR rainfall anomaly averaged over the region of 70°E-90°E, 10°N-30°N. This region is marked in Fig. 1n. SAS-ICE(Active: 5.37 mm/day, break: − 2.7 mm/day) is relatively close to the observation(Active: 5.36 mm/day, Break: − 4.0 mm/day). NSAS-NOICE shows a positive anomaly (0.32 mm/day) for the break period (Table 1), which is rectified in NSAS-ICE (− 1.84 mm/day).

Studies have pointed out that outgoing longwave radiation (OLR) is a useful parameter in the understanding of tropical circulations and considered as a reasonable indicator of convection (Murakami 1980; Prasad and Verma 1985; Krishnamurti et al. 1989; Chaudhari et al. 2010). Negative (positive)

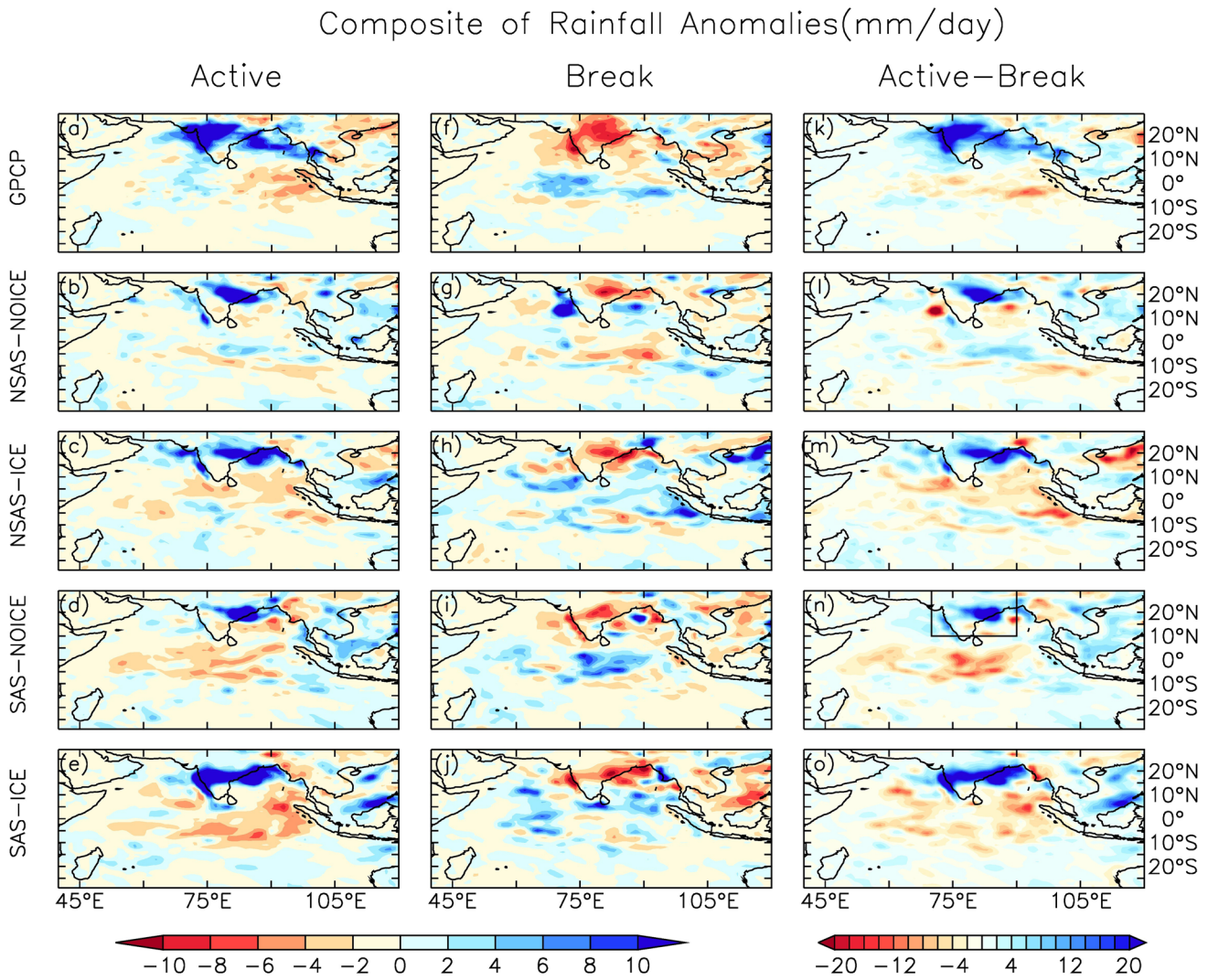

Fig. 1 Active (**a**–**e**) and break (**f**–**j**) composites of rainfall anomalies (mm/day) for GPCP, NSAS-NOICE, NSAS-ICE, SAS-NOICE, and SAS-ICE are presented. Difference between active and break composites (**k**–**o**) are also presented for GPCP, NSAS-NOICE, NSAS-ICE, SAS-NOICE and SAS-ICE, respectively

Table 1 Different parameters (viz. rainfall anomaly, OLR, specific humidity, upper-level cloud condensate) averaged over ISMR (70° E–90° E, 10° N–30° N) region of four model sensitivity experiments (NSAS-NOICE, NSAS-ICE, SAS-NOICE, and SAS-ICE) and observations for active and break phase

Active (break) [averaged over ISMR(70° E–90° E, 10° N–30° N) region]					
Parameters	Sensitivity experiments				Observations (GPCP, NOAA) reanalysis (MERRA)
	NSAS-NOICE	NSAS-ICE	SAS-NOICE	SAS-ICE	
Rainfall anomaly (mm/day)	2.62 (**0.32**)	3.66 (**− 1.84**)	2.48 (**− 1.95**)	5.37 (**− 2.70**)	5.36 (**− 4.01**)
OLR (W/m^2)	249.5 (**258.4**)	217.4 (**250.9**)	251.8 (**263.1**)	220.8 (**255.3**)	200.9 (**232.4**)
Specific humidity averaged over (300–800 hPa) (g/kg)					
Average	4.3 (3.9)	4.4 (3.5)	4.2 (3.8)	4.7 (3.6)	5.7 (4.6)
$\frac{(Active-break)}{active} \times 100\%$	9.30	20.45	9.50	23.40	19.30
Cloud condensate averaged over upper level (100–400 hPa) (mg/kg)	3.53 (2.55)	21.03 (9.05)	3.20 (1.72)	21.01 (7.93)	30.64 (20.07)

Values presented in parenthesis and marked by bold are for break phases

OLR anomalies are generally associated with strong (weak) convective activities.

During active spells, it is seen that the Indian land region and adjoining BoB region is marked by low values of OLR, which indicate strong convection over the region (Supplementary Fig. 2a). However, in the case of NOICE runs (i.e., NSAS-NOICE, SAS-NOICE; Supplementary Fig. 2b, d), a relatively higher amount of OLR as compared to observation is seen over Indian land region and adjoining BoB which indicate weaker convection over the region. On the other hand, NSAS-ICE and SAS-ICE simulated patterns of OLR are relatively closer to the observation for active (Supplementary Fig. 2c, e) as well as break spells (Supplementary Fig. 2h, j). As NOICE run contains only warm microphysics and ICE run contains both warm and cold phase microphysics, the response to OLR significantly varies according to the sets of experiments. Among the sensitivity experiments, simulations with NSAS-ICE show relatively better patterns of OLR over the Indian region. SAS-ICE run also stands good in the context of convection regions over Indian landmass. OLR averaged over the ISMR region (Table 1) does not depict significant variations in terms of active (NSAS-NOICE: 249.5 W/m^2; SAS-NOICE: 251.8 W/m^2) and break (NSAS-NOICE: 258.4 W/m^2; SAS-NOICE: 255.3 W/m^2) spells for NOICE runs. This hiccup is improved after incorporation of ice phase microphysics i.e., for both SAS-ICE (active: 220.8 W/m^2, break: 255.3 W/m^2) and NSAS-ICE(active: 217.4 W/m^2, break: 250.9 W/m^2). In a nutshell, the modulation of OLR (depiction of convection) is well captured by ICE phase microphysics for active and break composites. In contrast, insignificant variation is seen with NOICE run (i.e., warm phase microphysics). The improved simulation of OLR may be attributed to the better vertical profile of cloud condensate (discussed in Sect. 4.3) as OLR depends on cloud top temperature and cloud height. Hence incorporation of ice phase microphysics will improve the convection, which may lead to an improvement in MISO through the formation of stratiform clouds that regulates the latent heat release and helps to form intense depressions with enhanced precipitation (e.g., Choudhury and Krishnan 2011; Hazra et al. 2017a).

4.2 Moisture content

It is found that an increase or decrease of heavy precipitation is consistent with the enhanced or reduced tropospheric specific humidity, which can also be a functional predictor for rainfall extremity (Turner and Slingo 2008). It is also essential to represent the vertical and horizontal structure of humidity accurately in global circulation models to avoid resulting biases in radiative impact, which may affect the monsoon circulation (Gettelman et al. 2006). Udelhofen and Hartmann (1995) estimated that a 10% increase in upper tropospheric humidity might lead to ~ 1.4 W/m^2 of radiative forcing. Hence, it is essential to explore the possible potential differences in the humidity profile for ICE and NOICE simulations. Vertical profile of specific humidity (averaged over ISMR region of 70° E–90° E, 10° N–30° N) clearly shows the difference in these two types of simulation i.e., with and without ICE phase microphysics (Fig. 2). The difference in active and break composites of specific humidity is underestimated in both the NOICE simulations at pressure levels of 800–300 hPa, whereas the ICE simulations are relatively close with reanalysis (MERRA). While reanalysis based break composites have 19.3% less specific humidity (averaged over a region of 70° E–90° E, 10° N–30° N at 300–800 hPa) as compared to the active composites of the same region, NOICE simulations severely underestimate it by more than 50% (i.e., NSAS-NOICE: 9.3%; SAS-NOICE: 9.5%; see Table 1). It mostly gets improved by the incorporation of ice-phase microphysics (NSAS-ICE: 20.45%; SAS-ICE:23.4%), which is comparable with reanalysis (Table 1).

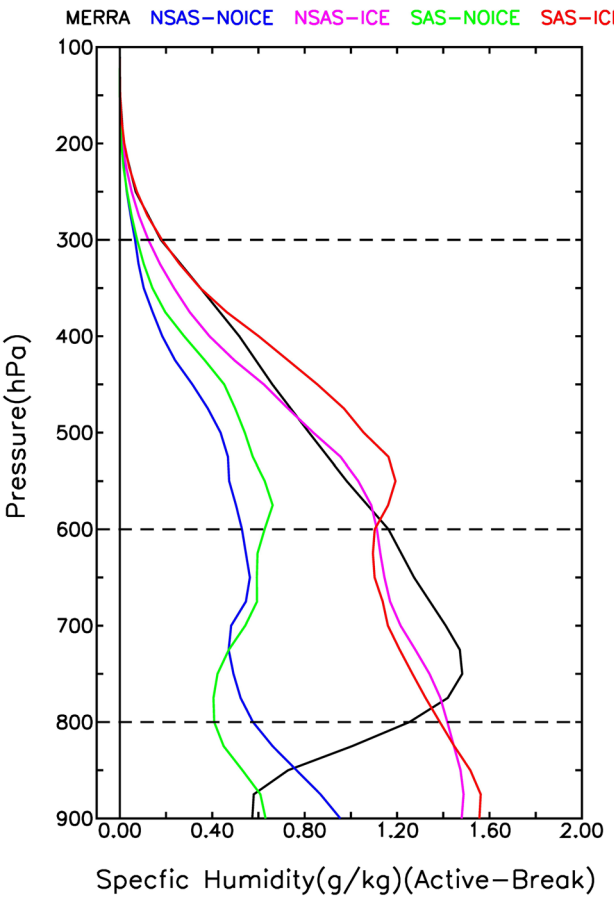

Fig. 2 Difference in vertical profile of specific humidity (g/kg) between active and break composites for MERRA (Reanalysis) and four sensitivity experiments for the region averaged over ISMR (70° E–90° E, 10° N–30° N)

The latitudinal distribution of the difference between active and break composites for the vertical profile of specific humidity (averaged over longitudes: 70° E–90° E) is presented in Fig. 3. Reanalysis product (MERRA) depicts a significant difference in specific humidity between active and break composites over the range of ISMR latitudes i.e., north to 10° N (Fig. 3). It has maximum differences over 20° N, across the pressure levels of 400–900 hPa. This feature is also validated with the NCEP2 (Kanamitsu et al. 2002) dataset (fig not shown), which reproduces similar results. NSAS-NOICE shows the differences over 20° N–30° N, but the maximum difference is only confined to lower tropospheric levels i.e., near 900 hPa, and for the higher levels, the difference is not significant. SAS-NOICE shows a similar kind of vertical orientation of the difference between active and break composites. Both the ice simulations (NSAS-ICE and SAS ICE) capture the variations in specific humidity between active and break spells at 15° N–25° N across the pressure levels (900–300 hPa), which is also reflected in the realistic representation of rainfall anomaly over Indian landmass region.

The longitudinal distribution of the difference between active and break composites for the vertical profile of specific humidity (averaged over latitudes: 10° N–30° N) is presented in Fig. 4. The difference in specific humidity over 70° E–90° E region (at pressure levels 900–300 hPa) is mostly

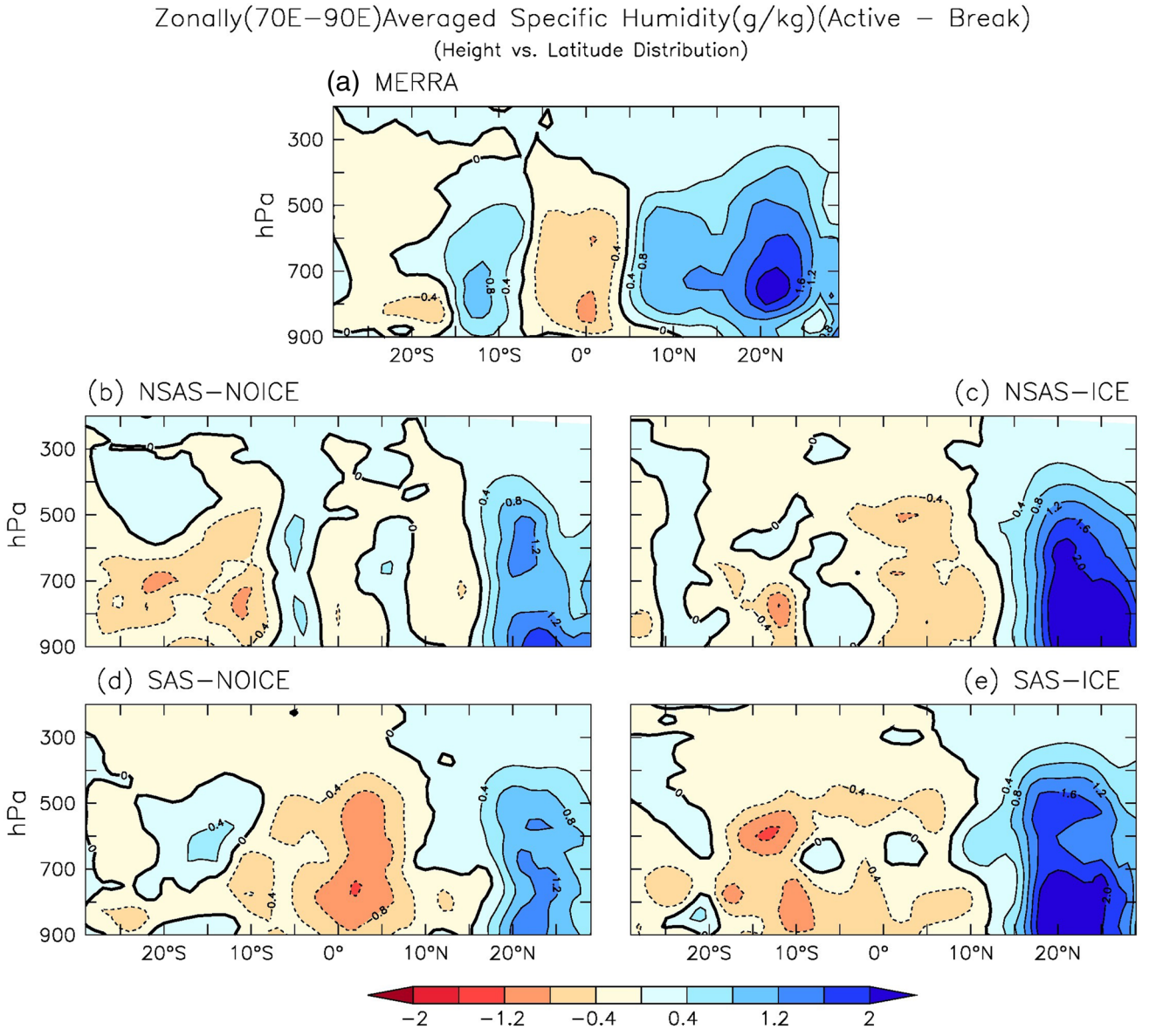

Fig. 3 Difference in height-latitude profile of zonally (70° E–90° E) averaged specific humidity (g/kg) between active and break for MERRA (reanalysis) and four model sensitivity experiments

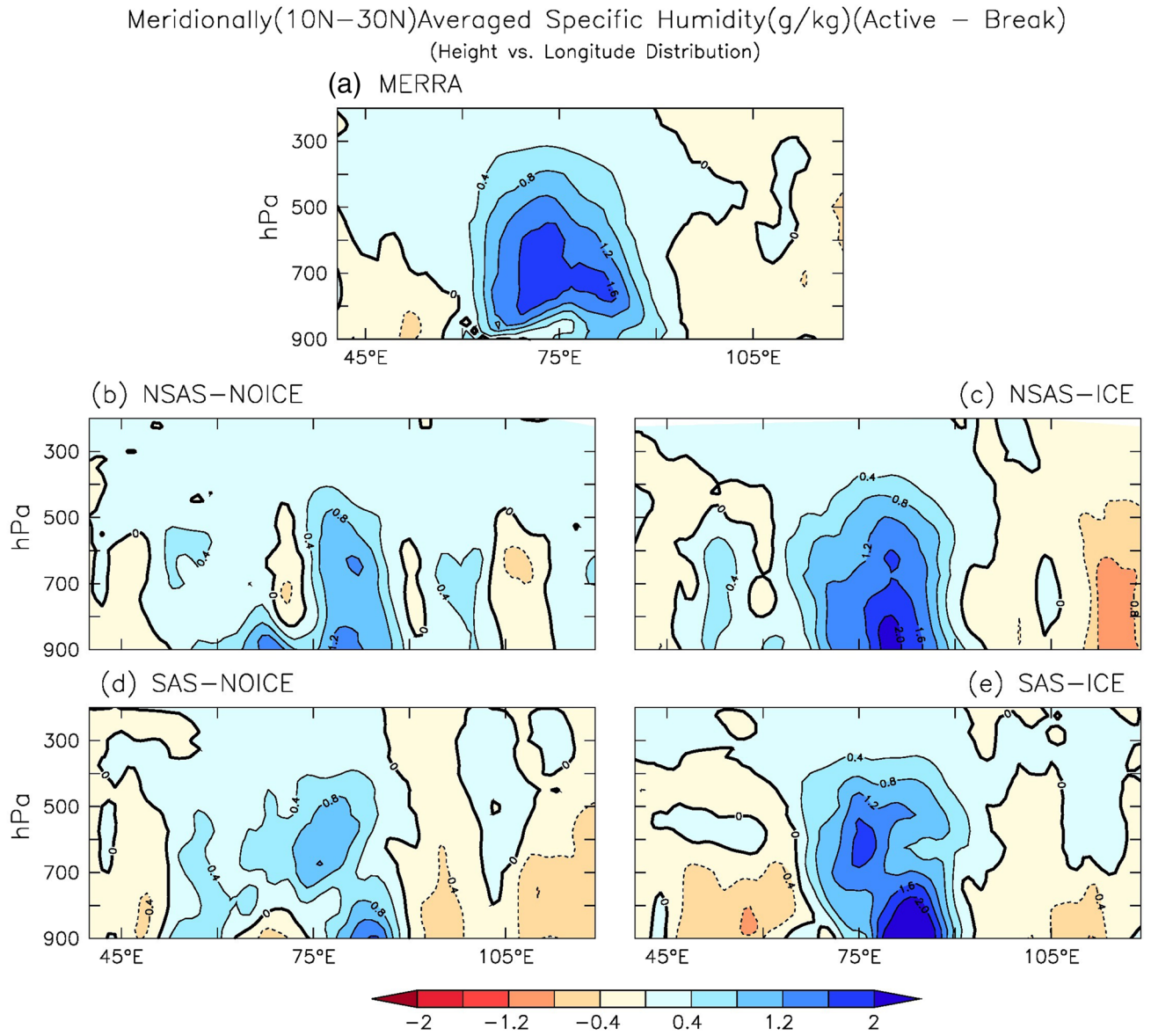

Fig. 4 Difference in height-longitude profile of meridionally averaged (over 10° N–30° N) specific humidity (g/kg) between active and break composites for MERRA (reanalysis) and four sensitivity experiments

underestimated by NOICE runs (Fig. 4b, d), which is considerably enhanced in the case of ICE runs (Fig. 4c, e).

Ice phase microphysical processes in the parameterization scheme realistically improve latent heating (LH) (Wang et al. 2010; Hazra et al. 2017a) by adding new sources and sink (Diao et al. 2017). As LH controls evaporative and condensation heating (Li et al. 2017) in the atmosphere, it has a substantial effect on water–vapor feedback (Cess 1989), which regulates the humidity of the atmosphere. Thus, it implies that the mixed-phase microphysics (ICE run) may realistically improve the vertical profile of moisture content, i.e., humidity, which further may lead to the improvement of MISO prediction.

4.3 Cloud condensate

The active spell is characterized by above-normal convective (~5%) and Stratiform (~20%) precipitating cloud over the monsoon trough region (Saha et al. 2014b), which is responsible for the abundant stratiform precipitation during the active phase (Choudhury and Krishnan 2011). Tang and Chen (2006) also pointed out that a large amount of high cloud exists in the ISM region, which accounts as large as 65% of all cloud grids. So, the study of the vertical profile of the cloud during ISM is essential as it has a strong response to thermodynamical, dynamical, and hydrological processes (Hazra et al. 2017a). The difference of cloud condensate

between active and break spell at upper levels i.e., above 450 hPa is nearly absent for the NOICE runs over the ISMR region, whereas it comes out to be as large as 17–18 mg/kg (NSAS-ICE and SAS-ICE) for ICE runs near 250 hPa which is also validated with reanalysis datasets (Fig. 5). Reanalysis shows the presence of more upper-level cloud condensate (100–400 hPa) in active spell (30.64 mg/kg) as compared to break spells (20.07 mg/kg; see Table 1). On the other hand, both the NOICE runs capture very less amount of cloud condensate (Table 1) in active spell (NSAS-NOICE: 3.53 mg/kg; SAS-NOICE: 3.21 mg/kg) as well as in break spells (NSAS-NOICE: 2.55 mg/kg; SAS-NOICE: 1.72 mg/kg). As we change the parameterization from NOICE run to ICE run, the upper-level cloud condensate improves realistically for the active and break spells. As a result, the difference between active and break also improves. SAS-ICE shows 21.01 (7.93) mg/kg for active(break) spell and NSAS-ICE also shows similar amounts i.e. 21.03 (9.05)mg/kg (Table 1). It is also seen that the difference in upper-level cloud condensate is maximum over the Indian land region, which is absent in both the NOICE runs (Supplementary Fig. 3b, d). It is realistically simulated in both the ICE runs, while SAS-ICE is better for the region over the Arabian Sea and West coast of India (Supplementary Fig. 3e) as compared to the reanalysis (Supplementary Fig. 3a).

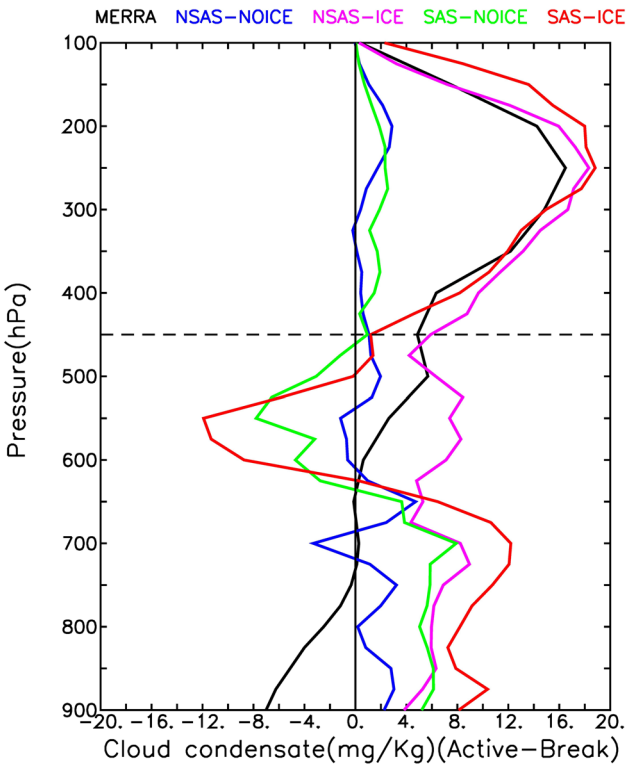

Fig. 5 Vertical profile of difference in cloud condensate (mg/kg) between active and break composites for MERRA (reanalysis) and four sensitivity experiments for the region averaged over ISMR (70° E–90° E, 10° N–30° N)

The latitudinal distribution of the difference between active and break composites for the vertical profileof cloud condensate (averaged over longitudes: 70° E–90° E) is better simulated (at 10° N–20° N) in ICE runs as compared to NOICE runs (Supplementary Fig. 4) for upper levels. Similarly, the longitudinal distribution of the difference between active and break composites for the vertical profile of cloud condensate (averaged over latitudes: 10° N–30° N, Supplementary Fig. 5) also shows similar kinds of results and indicates relatively better simulation by ICE runs.

As the ICE run simulates better specific humidity profile, better simulation of upper-level cloud condensate is expected. The cloud exists when the specific humidity is above the saturation specific humidity (Quaas 2012) at the corresponding temperature. A recent study by Baisya et al. (2018) also revealed that lack of moisture content in the tropospheric levels underestimates the cloud content (convective as well as stratiform). ICE run improves the vertical profile of specific humidity (Sect. 4.2), which is responsible for moisture content in the atmosphere. Ice microphysics also intensifies both updrafts and downdrafts (Straka and Anderson 1993) in the atmosphere. Further, it influences the vertical structure of the atmosphere and dynamic field (Li et al. 2017; Zhang 1989; Tao and Simpson 1989). Therefore, mixed-phase microphysics (ICE run) may realistically improve the cloud condensate vertical profile in active and break periods.

4.4 Lower and upper tropospheric circulations

The dominant feature of Indian monsoon circulation is characterized by a strong low-level southwesterly jet (Findlater jet), which peaks at around the Somali coast and Arabian Sea region (Wind patterns at 850 hPa; Fig. 6). South Westerly Jet (SWJ) connects the Mascarene high and Indian monsoon trough and forms the lower branch of the monsoon Hadley cell. In this perspective, it is important to explore the lower tropospheric features for active and break composites. It is seen that the conspicuous feature of SWJ core is stronger (weaker) in case of active (break) composites of winds at 850 hPa, which indicates an influx of moisture over the Indian region during active composites (Fig. 6a; MERRA). Model sensitivity experiments with ice (NSAS-ICE, SAS-ICE) are particularly good at capturing these observed features (Fig. 6a; MERRA) as compared to model runs with NOICE run. In case of break composites, interestingly, both ICE (NOICE) runs tend to underestimate (overestimate) the SWJ as in Fig. 6h, j (Fig. 6g, i). Overall, model sensitivity experiments with ICE run have a slightly better simulation of lower tropospheric circulation patterns and might represent better

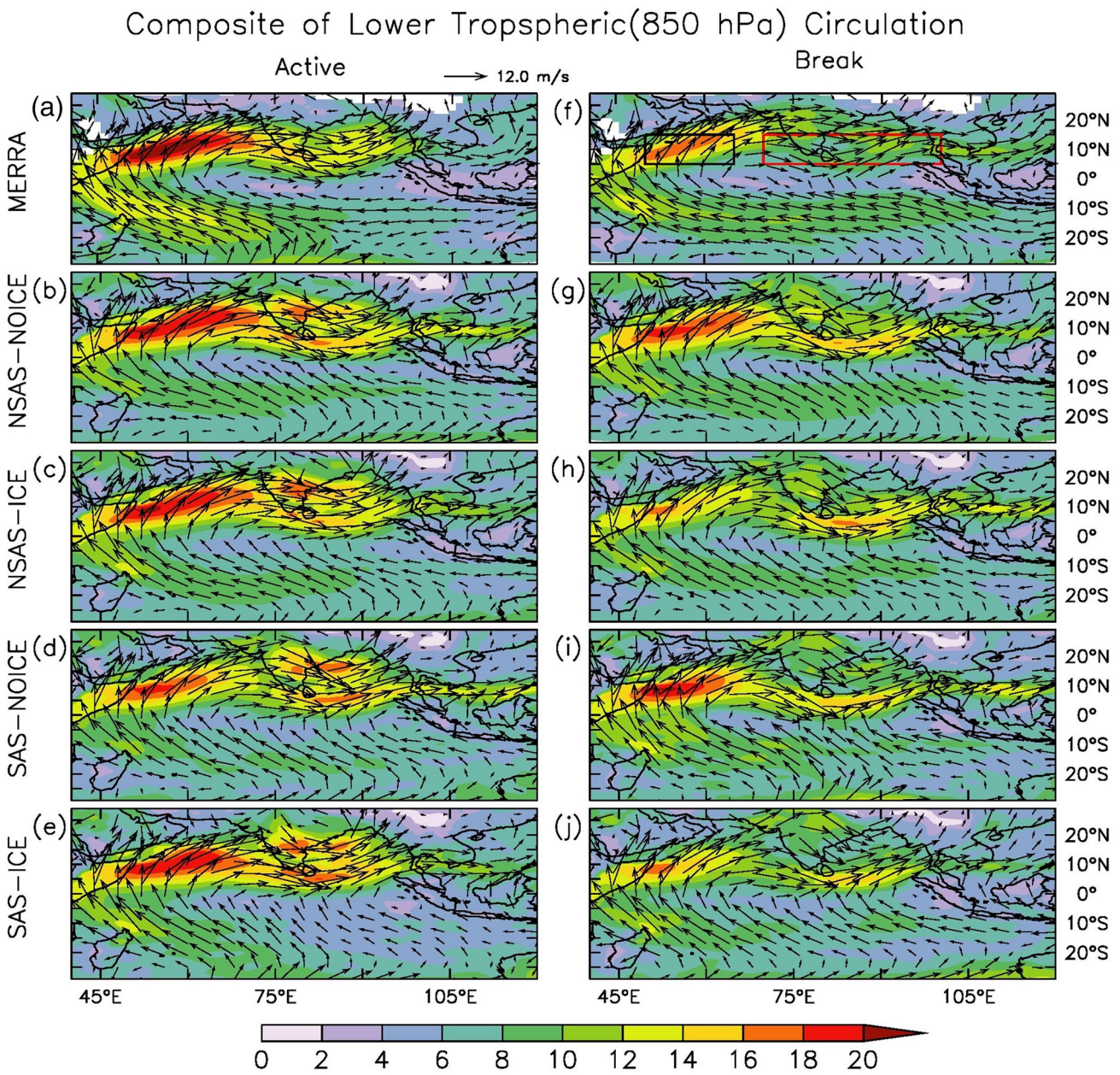

Fig. 6 Active (**a**–**e**) and break (**f**–**j**) composites of lower level wind (at 850 hPa) patterns (unit: m/s) for MERRA (reanalysis), NSAS-NOICE, NSAS-ICE, SAS-NOICE, and SAS-ICE respectively

rainfall patterns. Sometimes, dynamic instability of the SWJ may lead to a split of the jet near Somalia, creating two jets over India–Sri Lanka longitudes (Thompson et al. 2008). This splitting of the jet is considered as a temporary feature associated with break spell (e.g., Joseph and Sijikumar 2004). Interestingly, the dominance of the northern part of the SWJ (over a land region of Indian latitudes) is seen in the case of active composites of winds at 850 hPa (Fig. 6a–e). Similarly, the dominance of the southern part of the SWJ over the Bay of Bengal is marked by drier (weaker) monsoon during break composites (Fig. 6f–j). It is also in agreement with the theory proposed by Thompson et al. (2008).

To get a quantitative estimate of the improvement in low-level jet (Table 2a) we have chosen two boxes as b1 (50° E–65° E, 5° N–15° N) and b2 (70° E–100° E, 5° N–15° N), based on previous studies (Wilson et al. 2018; Viswanadhapalli et al. 2019, Joseph and Sijikumar 2004, etc.). The b1(b2) box is shown in Fig. 6f with black(red) outlines. We calculated the average wind speed in active and break composites along with pattern correlation (map to map correlation: Lund 1963; Kulkarni and Kriplani 1998; Hazra et al.

Table 2 (a) Quantitative comparison for lower tropospheric (850 hPa) circulation during active and break phase, (b) Quantitative comparison for upper tropospheric (150 hPa) circulation during active and break phase, (c) Monsoon-Hadley (MH) Index for active and break phase

Datasets (reanalysis and sensitivity experiments)	Region box	Box Average Value(m/s) (Pattern Correlation with MERRA)		$\frac{Active-break}{active} \times 100$
		Active	Break	
(a)				
MERRA (reanalysis)	b1: 50 E–65 E, 5 N–15 N	17.31	13.70	20.85
	b2: 70 E–100 E, 5 N–15 N	12.3	9.11	25.93
NSAS-NOICE	b1: 50 E–65 E, 5 N–15 N	16.70 (**0.96**)	15.70 (**0.75**)	5.99
	b2: 70 E–100 E, 5 N–15 N	12.93 (**0.71**)	11.68 (**0.42**)	9.67
NSAS-ICE	b1: 50 E–65 E, 5 N–15 N	16.52 (**0.98**)	12.61 (**0.86**)	23.67
	b2: 70 E–100 E, 5 N–15 N	12.87 (**0.87**)	11.17 (**0.49**)	13.21
SAS-NOICE	b1: 50 E–65 E, 5 N–15 N	14.83 (**0.95**)	15.81 (**0.70**)	− 6.61
	b2: 70 E–100 E, 5 N–15 N	12.51 (**0.33**)	10.12 (**0.11**)	19.10
SAS-ICE	b1: 50 E–65 E, 5 N–15 N	16.71 (**0.94**)	12.76 (**0.76**)	23.64
	b2: 70 E–100 E, 5 N–15 N	13.39 (**0.87**)	9.60 (**0.46**)	28.30

Datasets (reanalysis and sensitivity experiments)	Box average value (m/s) (pattern correlation with MERRA)		$\frac{Active-break}{active} \times 100$
	Active	Break	
(b)			
MERRA (reanalysis)	26.0	24.13	7.19
NSAS-NOICE	27.8 (**0.91**)	23.1 (**0.73**)	16.91
NSAS-ICE	26.1 (**0.91**)	20.7 (**0.71**)	20.69
SAS-NOICE	22.9 (**0.66**)	19.5 (**0.74**)	14.85
SAS-ICE	24.2 (**0.81**)	18.07 (**0.72**)	25.33

Datasets (reanalysis and sensitivity experiments)	MH-Index value		Active-break
	Active	Break	
(c)			
MERRA (reanalysis)	4.07	2.19	1.88
NSAS-NOICE	2.59	2.96	− 0.37
NSAS-ICE	4.0	0.34	3.66
SAS-NOICE	3.3	0.6	2.7
SAS-ICE	3.23	0.3	2.93

Values presented in parenthesis and marked by bold are 'pattern correlation' value of sensitivity experiments with reanalysis (MERRA)

2016) coefficient (PCC) of respective sensitivity experiments with reanalysis data (MERRA) in each box. We can see that the wind speed decreases by 20.85% (25.93%) in box b1(b2) from active phase to break phase for the reanalysis. NSAS-NOICE feebly captures this decrement while SAS-NOICE rather shows an increment of wind speed in (b1). NSAS-ICE can capture the decrement in box (b1) (23.67%) but underestimates the same in box (b2) (13.21%). SAS-ICE captures the same in b1(b2) 23.64% (28.30%), which is realistically closer than any other simulations. As per PCC is concerned, all the simulations show well (around 0.95) association with reanalysis for box (b1) during active phase. During the break for the same box, the PCC is higher in ICE-run (NSAS-ICE: 0.86, SAS-ICE: 0.76) than the respective NOICE-runs (NSAS-NOICE:0.75, SAS-NOICE: 0.70). Similar trends in PCC are also observed in the box (b2) but with more prominence, especially for SAS simulations. SAS-ICE shows much improvement in PCC [0.87(0.46)] for active (break) than SAS-NOICE [0.33(0.11)]. PCC of NSAS-ICE [0.87(0.49)] is similar to SAS-ICE in this box too.

Tibetan anticyclone encompasses an easterly jet stream in its southern flank, usually referred to as Tropical Easterly Jet (TEJ), located between 100 and 200 hPa. TEJ is located over southern India and adjoining the equatorial Indian Ocean. The wind at 150 hPa, which is considered as the core of the TEJ (Nithya et al. 2017) has been studied as an important parameter for Indian Summer Monsoon in many previous studies (e.g. Naidu et al 2011; Krishnan et al. 2009; Raju et al. 2005). The TEJ maximum is associated with the strength of the anticyclone (e.g., Hazra et al. 2015). As a

result, the strength of TEJ is linked with the monsoon activity over the Indian subcontinent (Chaudhari et al. 2016a). Stronger (weaker) TEJ during active (break) composites indicate strong (weak) monsoon (Fig. 7a, f; MERRA). Model experiments are also able to depict these conspicuous features, although it has variations in terms of magnitude. Active composites of winds at 150 hPa for most of the sensitivity experiments indicate that TEJ is strongest over the southern Indian Ocean and adjoining oceanic regions. Among all experiments, both the SAS-simulations during both active and break composites are relatively weaker as compared to observation and NSAS-simulations (Fig. 7e, j, Table 2b).

Similarly quantitative estimate (Table 2b) for Tropical Easterly Jet (150 hPa) is performed over box (b3) 50° E–100° E, 10° S–15° N (e.g. Abish et al. 2013) (blue box in Fig. 7a, f). All the simulations overestimate the decrement in wind speed from active to break composites. However, it is seen that the decrement is more in ICE-run (NSAS-ICE: 20.69%, SAS-ICE: 25.33%) as compared to the respective NOICE-run (NSAS-NOICE: 16.91%, SAS-NOICE: 14.85%). For Break composite, PCC is nearly the same for

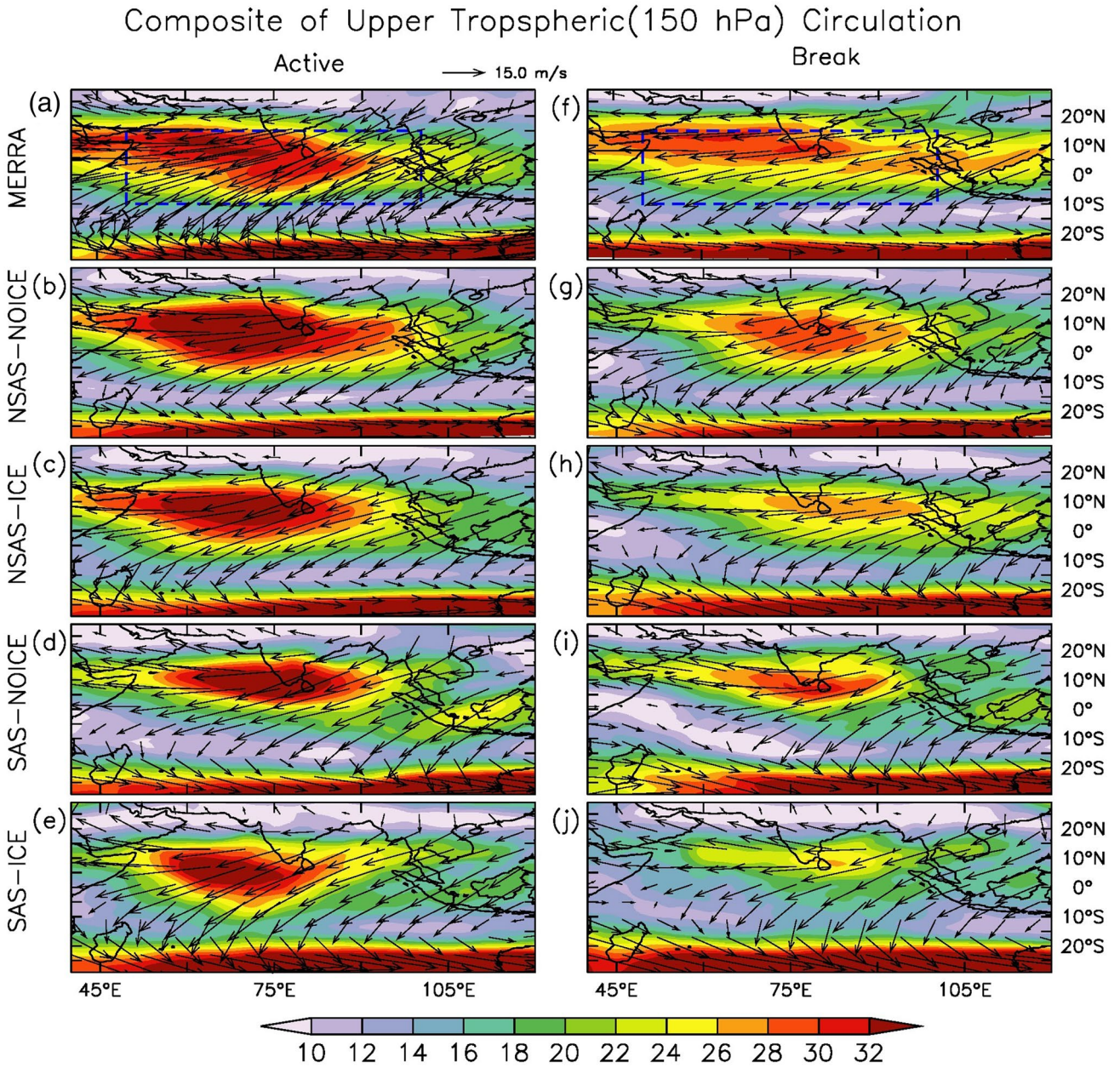

Fig. 7 Active (**a**–**e**) and break (**f**–**j**) composites of upper level wind (at 150 hPa) patterns (unit: m/s) for MERRA, NSAS-NOICE, NSAS-ICE, SAS-NOICE and SAS-ICE respectively

all simulations. However, for active composite, PCC is considerably more in SAS-ICE (0.81) than SAS-NOICE (0.66).

We have presented the Monsoon-Hadley (MH) index (Table 2c), which is positively correlated with the strength of the Indian Summer Monsoon (Goswami et al. 1999) for active and break composites. It is calculated as follows

$$\text{MH - Index} = V_{850\ \text{hPa}} - V_{200\ \text{hPa}}$$

where V is the meridional component of wind averaged over 70° E–110° E, 10° N–30° N.

NSAS-NOICE incorrectly shows the MH-Index more in break phase (2.96) than active phase (2.59), which is corrected by NSAS-ICE (active: 4.0, break: 0.34). Both the SAS simulations are able to capture MH-Index realistically. However, the difference (active minus break) is more in SAS-ICE (2.93) than SAS-NOICE (2.7).

All these results pinpoint that ICE-run (NSAS-ICE and SAS-ICE) can capture the difference in circulation pattern between active and break phase more prominently, which results in better simulation of the active-break phase.

4.5 Hadley and Walker circulation

The Indian summer monsoon is mostly a superposition and interaction between a regional Hadley circulation and a planetary scale Walker circulation (Goswami 1994; Goswami et al. 1999). In this context, it is vital to find the possible role of ice-processes on these two significant circulations on the intraseasonal time scale (active-break cycle) of the ISMR.

4.5.1 Regional Hadley circulation

Regional anomalous Hadley (averaged over 70° E–90° E) circulation for four sensitivity experiments (ICE and NOICE run along with SAS and NSAS) are presented in Fig. 8. The pressure vertical velocity (omega) is considered here for the representation of the features of Hadley circulation. Positive (negative) omega sign indicates the descending (ascending) branch of the Hadley circulations. During the active condition, a distinct descending (ascending) branch is observed south (north) of 15° S along with a low level (surface to 500 hPa) descending branches near the equator (Fig. 8a). Both ascending and descending branches in all four sensitivity experiments are simulated with major changes in the width and extent of these branches as compared to MERRA. Both NSAS-NOICE and NSAS-ICE run have good simulation of ascending branches of Hadley circulation. Further, the NSAS-NOICE scheme indicates a stronger descending branch as compared to observation in active condition (Fig. 8b), thus NSAS-ICE is comparatively better as compared to NSAS-NOICE. However, both SAS-NOICE and SAS-ICE can capture the position of the strong ascending branch over the Indian region during the Active phase with marginal differences between them.

Similarly, during break condition, the distinct descending branch is seen over the south of 15°S and ascending branch over the north of 10° S. It is relatively less intense as compared to that of active composites (MERRA; Fig. 8a, f) as break period is known to be associated with an increase in equatorial convection, also referred to as southward shift of ITCZ (e.g., Sikka and Gadgil 1980). As a result, weak rising motion is seen over the Indian region, which is indicative of less rainfall. NSAS-NOICE scheme (Fig. 8g) is not able to capture this feature in contrast with the other three schemes. During break composites, NSAS-NOICE simulates a stronger ascending branch, unlike in the reanalysis dataset (here MERRA), which may lead to more rainfall simulation over the Indian region (Fig. 8g). The same is rectified in NSAS-ICE (Fig. 8h). Overestimation of the ascending branch is also seen in the SAS-NOICE run near equator (Fig. 8i) which gets improved in SAS-ICE run (Fig. 8j). Overall, NSAS-ICE and SAS-ICE simulated Hadley circulation during both active and break conditions are in better agreement with observation as compared to other experiments.

4.5.2 Walker circulation

Walker circulation is dictated by the equatorial heat sources (e.g., Goswami 1994), and characteristics of the Walker Circulation are determined mainly by the coupling between the tropical atmosphere and oceans. Therefore, it is crucial to explore the Walker circulation patterns during active and break composites.

MERRA reanalysis depicts the ascending branch of Walker circulation over the Indian region during active and break composites (Fig. 9a, f). During the active spell, SAS-ICE simulated ascending branch over Indian landmass is relatively better simulated than other experiments (Fig. 9e). NOICE runs (NSAS-NOICE, SAS-NOICE) composites during active spells show an overestimation of ascending branch (especially at level 300–700 hPa) as compared to MERRA, which is further improved in ICE runs (NSAS-ICE, SAS-ICE). Similarly, for break composites, the ascending branch of Walker circulation is overestimated in the SAS-NOICE run (Fig. 9i) which is reduced in SAS-ICE (Fig. 9j).

Hence, simulation of both these circulations (Hadley and Walker) also highlight the requirement of more development and proper representation of ice processes in a coupled climate model.

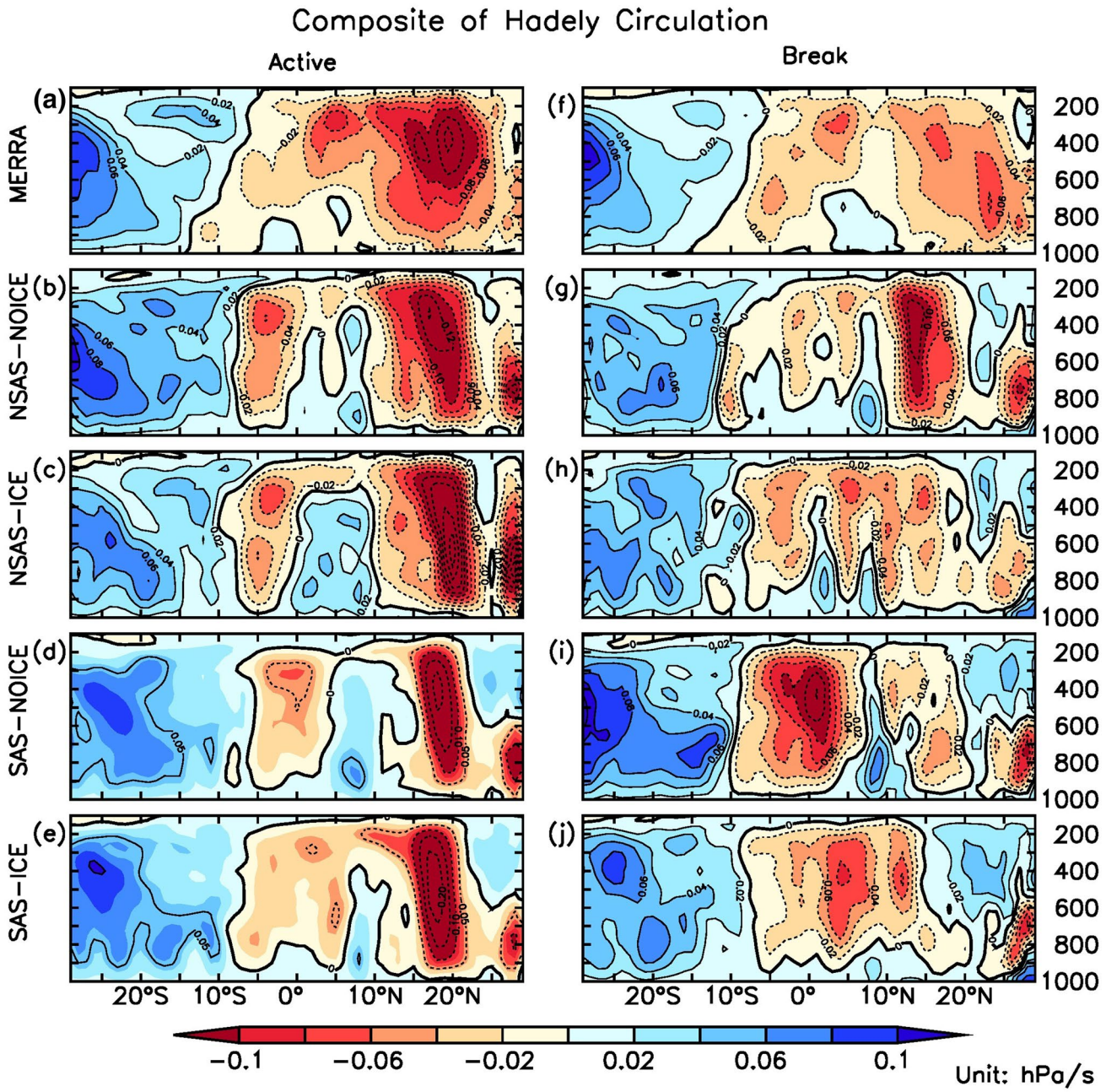

Fig. 8 Active (**a**–**e**) and break (**f**–**j**) composites of Hadley circulation (pressure vertical velocity averaged over 70° E–90° E) for MERRA, NSAS-NOICE, NSAS-ICE, SAS-NOICE and SAS-ICE respectively

5 Intraseasonal variability

A significant part of the interannual variance of seasonal-mean (averaged over June–September) rainfall is explained by the monsoon intraseasonal variability (Goswami 1998). The presence of active or break phase significantly modules precipitation along with the associated changes in the large-scale circulations. The monsoon intraseasonal variability has a dominant mode of periodicity in 10–20 days and 30–60 days (Murakami 1976; Krishnamurti and Bhalme 1976; Yasunari 1980; Sikka and Gadgil 1980; Rahman and Simon 2006). The 10–20 days band is a westward propagating mode and 30–60 days band is the northward propagating mode of ISOs. It will be interesting to investigate the various ISO features in different ice-phase microphysics experiments.

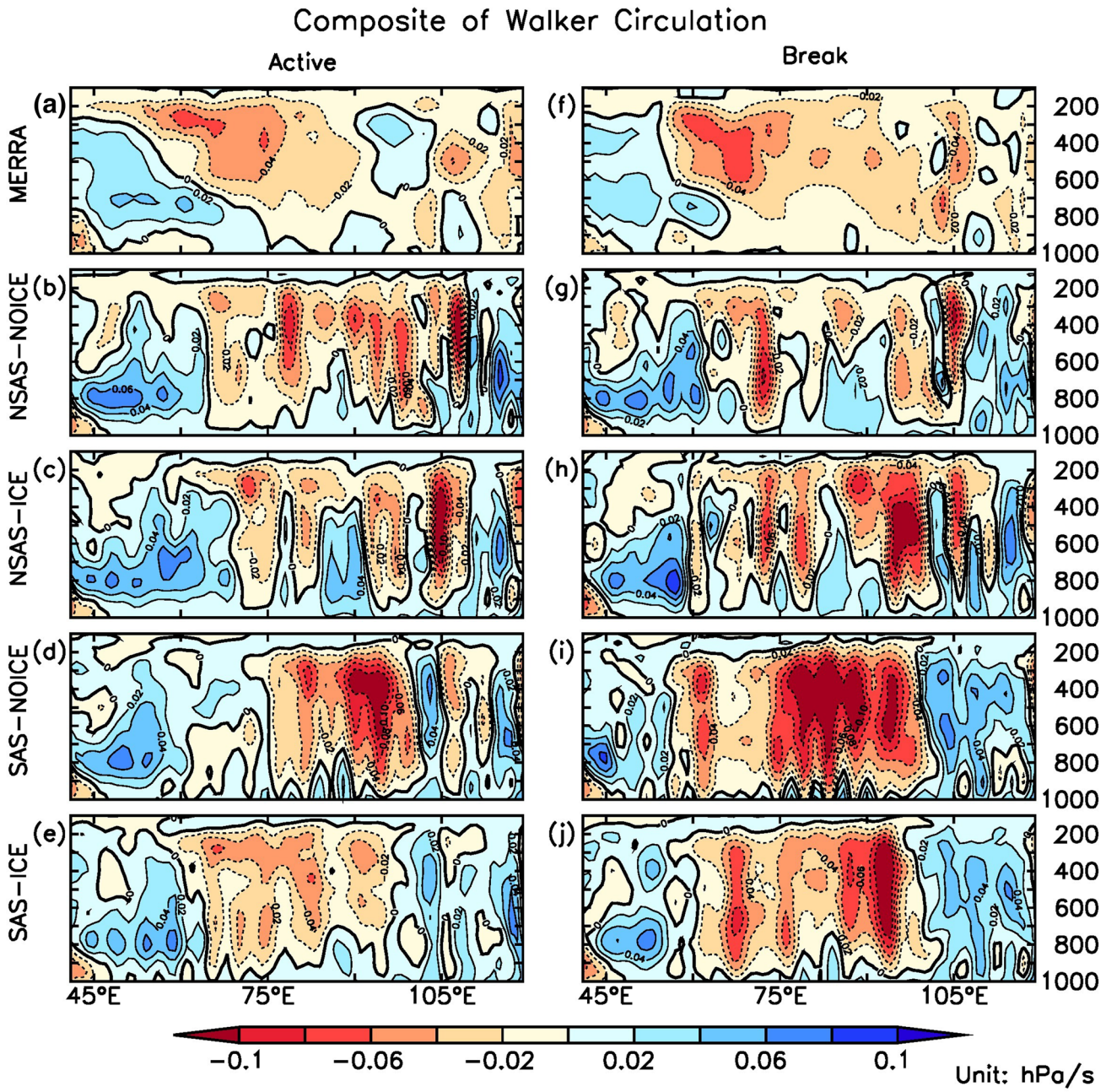

Fig. 9 Active (**a**–**e**) and break (**f**–**j**) composites of Walker circulation (pressure vertical velocity averaged over 5° S–5° N) for MERRA, NSAS-NOICE, NSAS-ICE, SAS-NOICE and SAS-ICE respectively

5.1 North–south space–time spectra of ISO band (20–100 days)

To examine the role of ice-phase microphysics in modulating the dominant modes of ISV, north–south space–time spectra of zonally averaged (60° E–110° E), filtered (20–100 days) daily rainfall anomalies (June–September) are presented in Fig. 10. The methodology of computation is based on Wheeler and Kiladis (1999). Here the meridional wavenumber 1 corresponds to the largest wave that will fit within the latitudinal extent (20° S–33° N) (Goswami et al. 2011). Period (days) on positive (negative) x-axis shows northward (southward) propagation (e.g. Hazra et al. 2017b; Saha et al. 2014c). The observations indicate that the most dominant mode of northward propagating ISO (located at wave number 1 with 40-day periodicity) is stronger than the southward counterpart (Fig. 10a). In general, all experiments can capture the more(less) power at northward (southward)

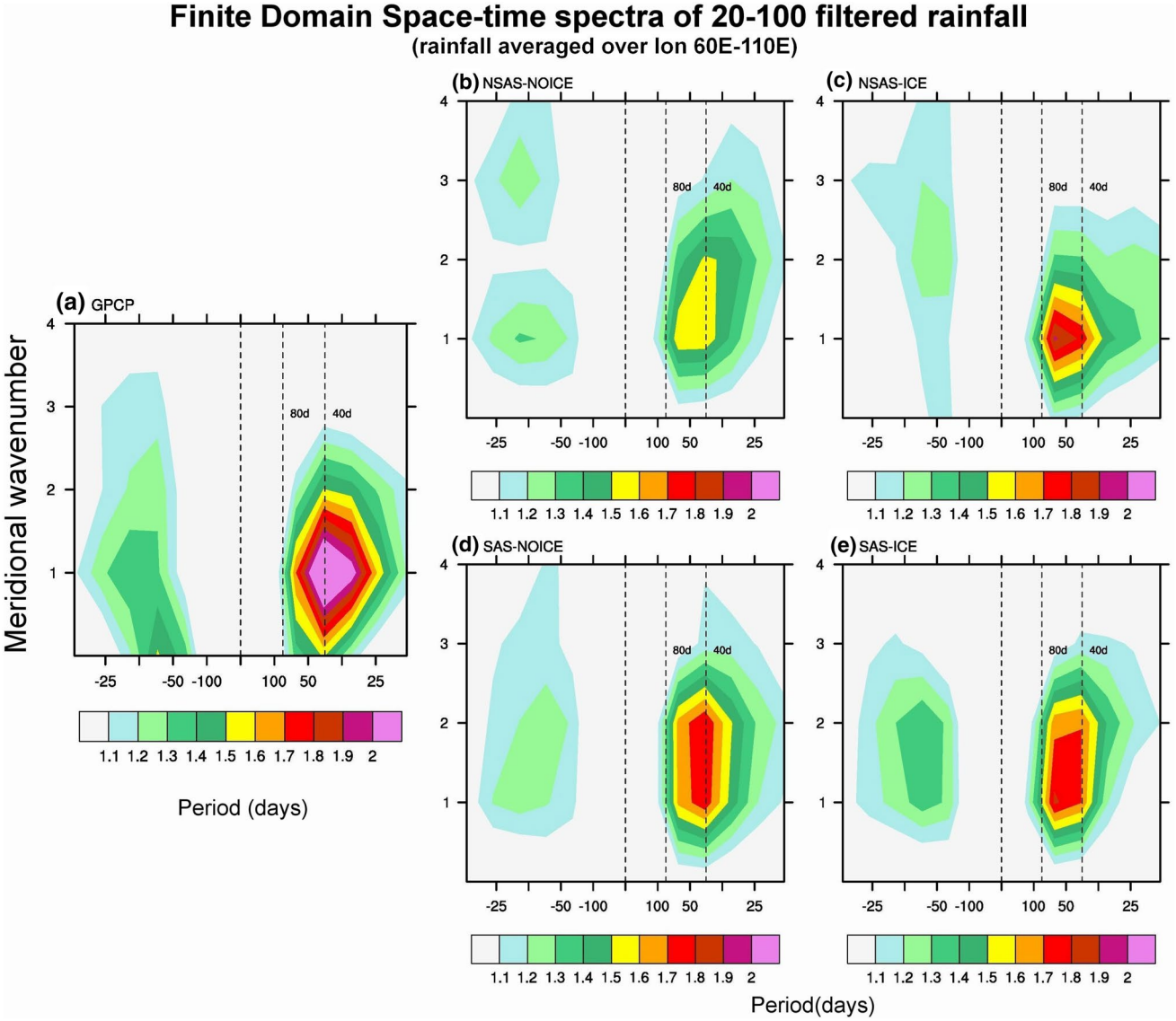

Fig. 10 North–South space time spectra for 20–100 day filtered rainfall anomaly (averaged over 60° E–110° E) for **a** GPCP, **b** NSAS-NOICE, **c** NSAS-ICE, **d** SAS-NOICE and **e** SAS-ICE respectively

propagating mode, as depicted in observation (Fig. 10b–e). In case of NSAS-NOICE (Fig. 10b), maximum power is highly underestimated at northward propagating mode as compared to observation, and the southward propagating mode is also not adequately simulated. As compared to NSAS-NOICE, SAS-NOICE is relatively better in terms of the amplitude of both northward and southward mode. However, the maximum power of northward propagating mode is still underestimated to some extent, and it is spread over wave numbers 1 and 2 (Fig. 10d). The southward propagating mode of NSAS-NOICE is also underestimated as compared to observation. Both NSAS-ICE and SAS-ICE runs are better than NOICE experiments both in terms of the amplitude of propagating (northward and southward) power and their wave number peaking. Among all of these experiments, SAS-ICE shows a better representation of the space–time spectra, which suggests that ice microphysics significantly modulates the ISO features. The results also indicate that the incorporation of ice-phase microphysics depicts realistic improvement for the NSAS scheme, which may be related to the nonlinear interaction between microphysics and convection as pointed out by Liu et al. (2018).

5.2 10–20 Day mode

The intraseasonal variance (ISV) of filtered 10–20 days rainfall anomaly for observation and sensitivity experiments are presented in Fig. 11a–e. Different convection schemes

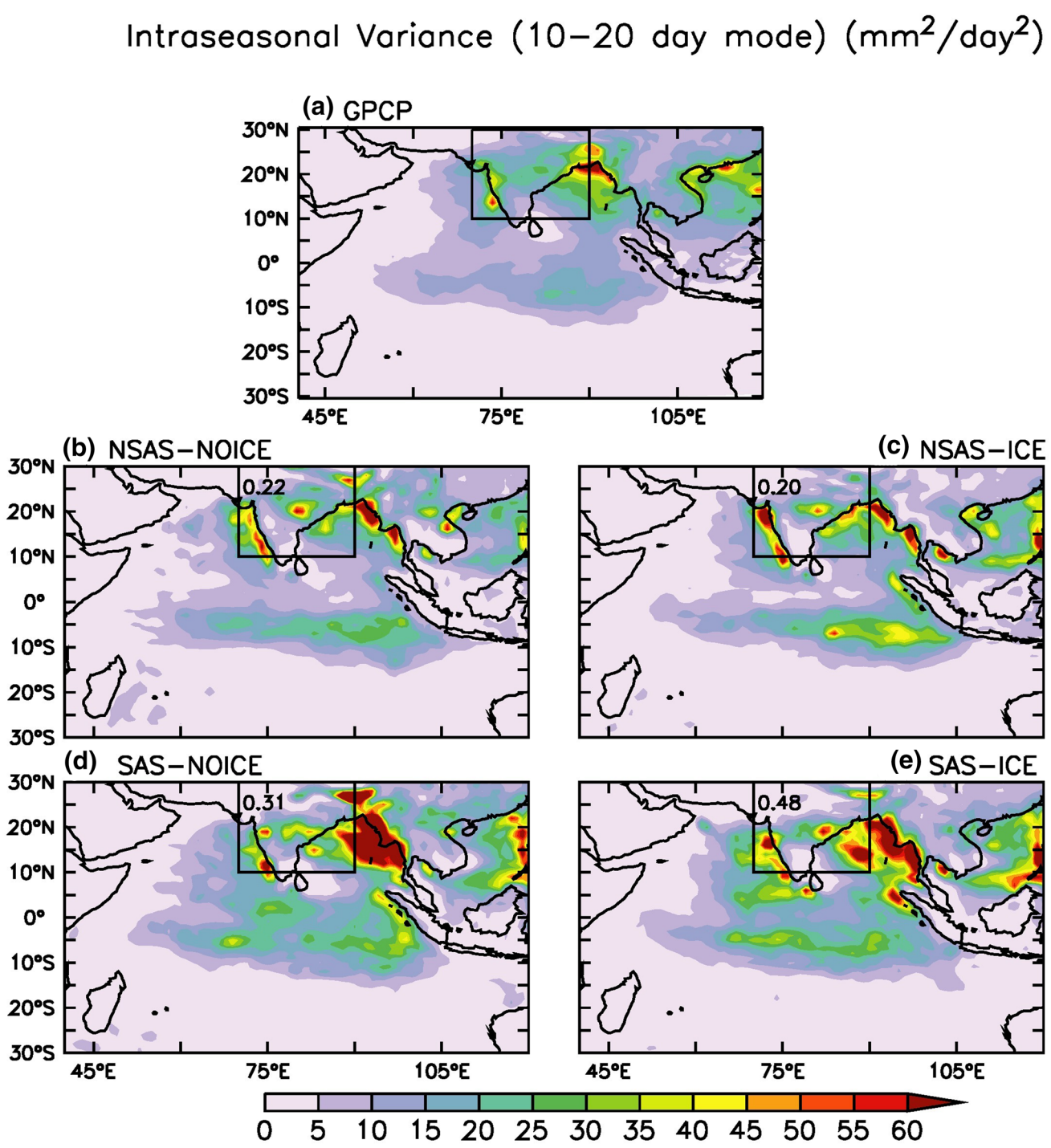

Fig. 11 The intraseasonal variance (ISV) of filtered 10–20 days rainfall anomaly for **a** GPCP, **b** NSAS-NOICE, **c** NSAS-ICE, **d** SAS-NOICE and **e** SAS-ICE respectively. Pattern correlation of all the sensitivity experiments with GPCP is written in ISMR box on each panel

(SAS and NSAS) and microphysics (warm and cold) have a significant impact on the pattern of ISV. All the sensitivity experiments largely overestimate the magnitude of variance over the West Coast of India, and at the same time, both SAS-NOICE and SAS-ICE largely overestimate the variance over northern BOB and the South China Sea as compared to NSAS schemes. To get a quantitative idea of the fidelity of the simulations pattern as compared to observation, we have calculated pattern correlation coefficient (PCC) for all the sensitivity experiments with the observation for the ISMR region (shown in box; see Fig. 11). SAS-ICE shows the highest PCC (0.48), which is double than that of NSAS-Schemes.

NSAS-NOICE (0.22) depicts marginally higher PCC than NSAS-ICE (0.20). It is also seen that both the SAS simulations (SAS-NOICE: 0.31, SAS-ICE: 0.48) show better PCC as compared to NSAS simulations.

The 10 to 20-day mode is associated with westward-moving disturbances from the western Pacific Ocean to the BoB (Murakami 1976; Krishnamurti and Bhalme 1976; Chatterjee and Goswami 2004). The propagation characteristics of 10–20 days mode for observations and sensitivity experiments are presented by lag-longitude (averaged over 10° N–20° N) diagram of regressed (lead/lag) 10–20 days filtered rainfall anomaly in Fig. 12a–e. Area averaged central India (74° E–83° E, 15° N–25° N) 10–20 days filtered rainfall anomaly is taken as a reference series for regression. The westward propagation in NSAS-NOICE (Fig. 12b) is not consistent as rain-bands becomes stationary (within the 85° E–95° E) and then propagate westward (West of 85°E), which gets slightly improved in NSAS-ICE (Fig. 12c). As we change the convective parameterization scheme from NSAS to SAS, the model simulated patterns of westward propagation get improved. Both SAS-NOICE and SAS-ICE simulations are relatively better in capturing the propagating features of westward propagation; however, amplitudes are overestimated (Fig. 12d, e). In the case of SAS-ICE, the propagation is more coherent, and also the magnitude is marginally overestimated. This suggests that convective coupling is more realistic in ice microphysics run, as the westward propagating mode of 10–20 day is in general driven by convective coupling (e.g., Chatterjee and Goswami 2004).

5.3 30–60 day Mode

The intraseasonal variance of 30–60 day mode is presented in Fig. 13a–e. Observation depicts a zone of high variance over the West coast of India and adjacent the Arabian Sea, northern Bay of Bengal and the South China Sea. Sensitivity experiments can capture the high variance zones, especially over the Western Ghats of India and over the relatively smaller portion of north Bay of Bengal. The variances are mostly aligned along the Myanmar coast. Both NSAS-NOICE and NSAS-ICE highly underestimate the ISO variance over the Bay of Bengal. SAS-NOICE and SAS-ICE are slightly better in capturing the observed variance (Fig. 13). SAS simulated experiments also captured the variance over the eastern equatorial Indian Ocean realistically (Fig. 13d, e). PCC (i.e., map–map correlation) analysis over the ISMR region yields no significant correlation for both the NSAS-schemes and even for that of SAS-NOICE. Interestingly SAS-ICE also performs better here with promising PCC of 0.35. It is seen that choice of convective parameterization scheme is of much importance for the realistic simulation of intraseasonal variance. However, it is good to see that a combination of the SAS scheme with mixed-phase microphysics has better aspects in this regard.

Lag-Latitude (averaged over 70° E–90° E) diagram (Saha et al. 2013; Goswami et al. 2011) of regressed (lead/lag) (region for reference series as mentioned in Sect. 5.2) 30–60 days filtered rainfall anomaly is presented in Fig. 14a–e. Both the SAS schemes can capture the northward propagation feature. SAS-ICE has performed better than SAS-NOICE.

6 Conclusions

This study has investigated the role of microphysics (i.e., warm and mixed-phase) in association with two different convection schemes for Indian summer monsoon ISO. This study emphasizes that the proper feedback between convective and microphysics processes plays an essential role in the better simulation of Monsoon Intraseasonal Oscillation (MISO) in CGCM.

In this study, four sensitivity experiments are carried out using coupled climate model- CFSv2 with two different combinations of convective parameterization (SAS and NSAS) and two different microphysics (with and without ICE microphysics). In general, for the case of active composites, NOICE runs (i.e., NSAS-NOICE, SAS-NOICE) fail to depict observed positive rainfall anomaly over Indian land and adjoining BoB regions. On the other hand, ICE included parameterization schemes (SAS-ICE and NSAS-ICE) that lead to a more realistic spatial rainfall pattern during the ISM season. SAS-ICE depicts relatively better results. The difference between ICE and NOICE run can be attributed to the availability of cloud condensate to the upper level in case of ICE run, which is absent in NOICE run. OLR composites are also closer to observation in ICE microphysics run, which is consistent with rainfall composites.

Lower tropospheric circulations are better represented by ICE microphysics run. SWJ is also better captured in ICE-run. The splitting of SWJ is also seen, and dominance of the northern part of the SWJ is seen in the case of active composites of winds at 850 hPa. Similarly, the dominance of the southern part of the SWJ over the Bay of Bengal is seen during break composites. These features are better captured by ICE microphysics run as compared to NOICE microphysics run. Upper tropospheric features, including TEJ, are also better captured by ICE microphysics run.

SAS-ICE run simulated Hadley circulation for active and break conditions are relatively in line with observation as compared to other experiments. NOICE runs composites during break spells show overestimation of ascending branch as compared to MERRA, which is relatively improved in ICE runs. SAS-ICE simulations are relatively better even though it has some differences with MERRA reanalysis.

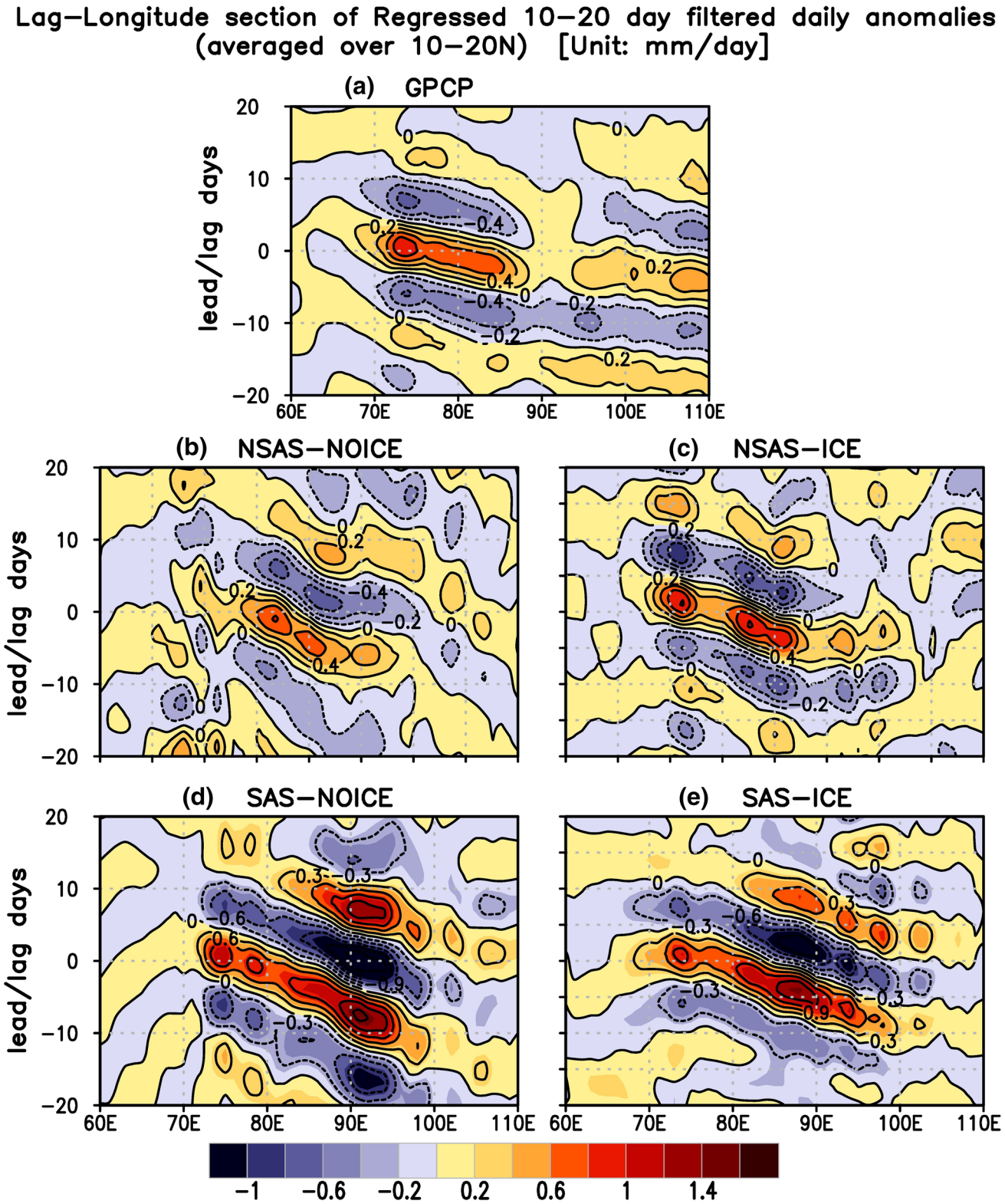

Fig. 12 Lag-Longitude (averaged over 10° N–20° N) diagram of regressed rainfall anomalies (10–20 days filtered) **a** GPCP, **b** NSAS-NOICE, **c** NSAS-ICE, **d** SAS-NOICE and **e** SAS-ICE

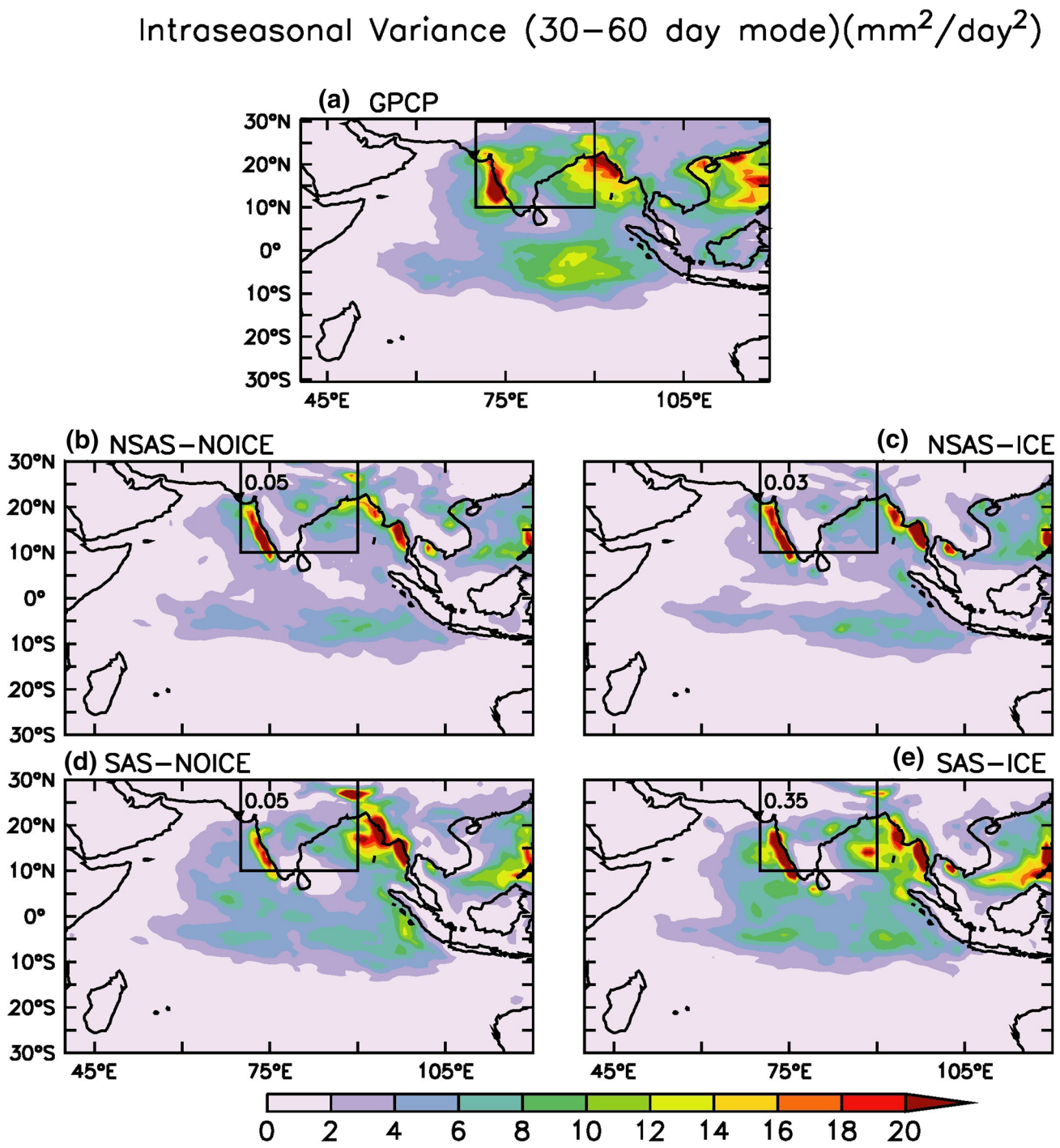

Fig. 13 The intraseasonal variance (ISV) of filtered 30–60 days rainfall anomaly for **a** GPCP, **b** NSAS-NOICE, **c** NSAS-ICE, **d** SAS-NOICE and **e** SAS-ICE respectively. Pattern correlation of all the sensitivity experiments with GPCP is written in ISMR box for each panel

SAS-ICE simulated Walker circulation during active spell composites denote ascending branch over Indian landmass, which is in relatively better agreement with observation as compared to other sensitivity experiments. NOICE runs (NSAS-NOICE, SAS-NOICE) composites during active spells depict the overestimation of ascending branch as compared to MERRA, which is further improved in ICE runs (NSAS-ICE, SAS-ICE).

The vertical profile of humidity is realistically improved in ICE-runs, which may result in better representation of temperature profile (Supplementary Fig. 6) during active and break composites. The temperature (averaged over

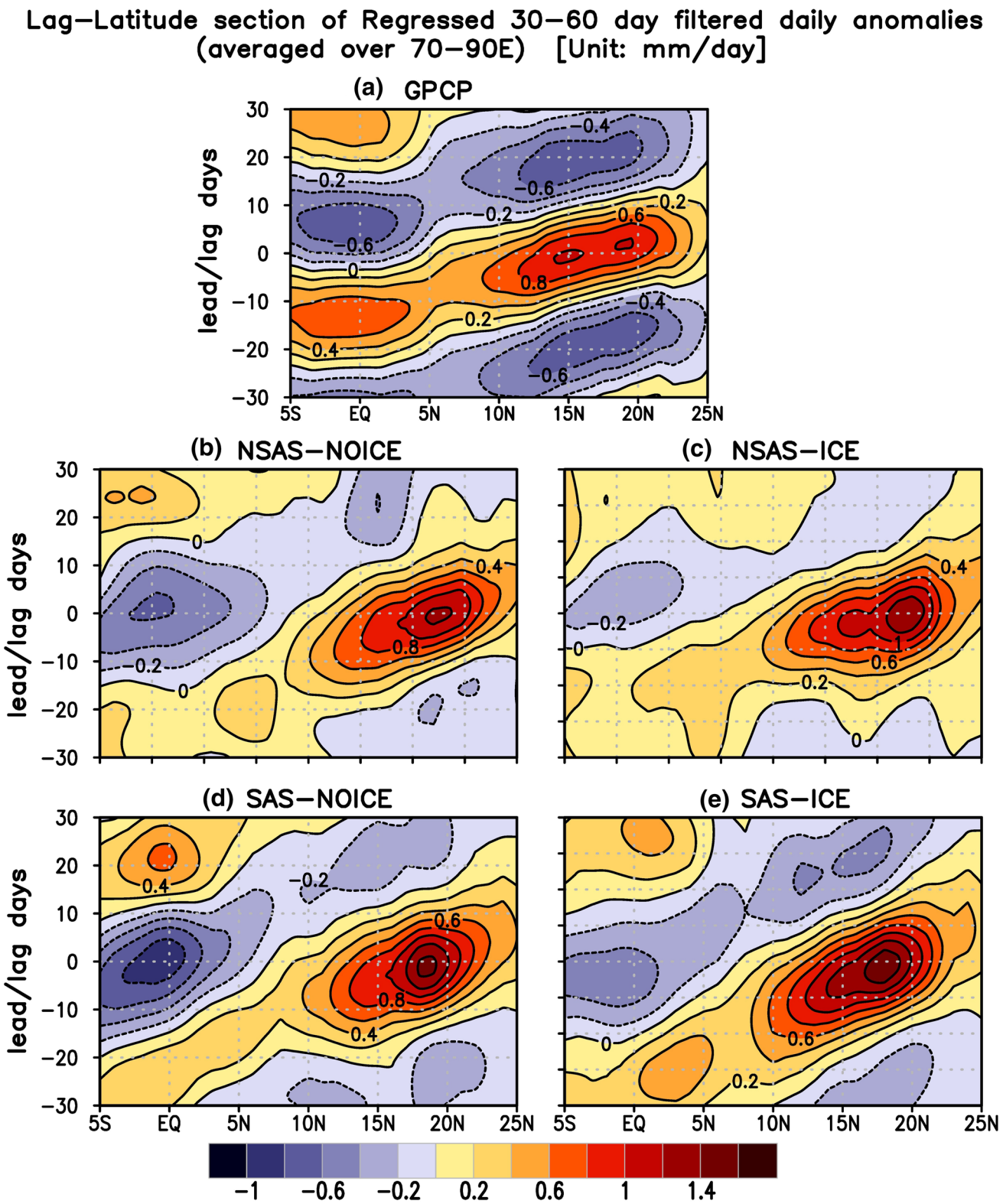

Fig. 14 Lag-Latitude (averaged over 70° E–90° E) diagram of regressed rainfall anomalies (30–60 days filtered) **a** GPCP, **b** NSAS-NOICE, **c** NSAS-ICE, **d** SAS-NOICE and **e** SAS-ICE

30° E–110° E, 15° S–35° N, Hazra et al. 2017a) bias for each simulation is mostly negative and the bias is more in the upper levels as compared to lower levels for both the scenario (active and break composites). However, in both cases, the negative bias is decreased (maximum about 2 °C) in ICE-runs for upper levels. SAS-ICE has the least bias among all the simulations. All these lead to the improvementin the circulation pattern in SAS-ICE-run.

In the case of intraseasonal oscillations, ICE runs (NSAS-ICE and SAS-ICE) show maximum power at northward propagating mode, which is improved as compared to NOICE runs and has close resemblance with observations. Sensitivity experiments can depict the northward propagating mode. ICE run (NSAS-ICE and SAS-ICE) experiments show northward propagating mode (30–60 day mode) of ISO, which is relatively better than NOICE microphysics experiments.

NSAS-NOICE fails to capture the westward propagation (10–20 day mode). SAS schemes depict relatively better performance over the equatorial Indian region. SAS-ICE simulations are superior in depicting the observed characteristics of westward propagation, implying convective coupling is getting stronger with ice microphysics run, and 10–20 day westward propagating mode gets improved. All of these results suggest that ICE microphysics parameterization has the utmost importance in the simulation of MISO.

Vertical profile of specific humidity is better simulated by the ICE microphysics, which plays a big role in convection and upper-level cloud formation through microphysical aspects (as discussed in Sect. 4.2). Upper-level cloud condensate also plays a great role in regulating the active-break spell, which is better simulated by ICE run. In contrast, the NOICE run fails to capture the upper-level cloud condensate. Moreover, as a result, it fails to capture the active and break composites.

Results reveal that ice-phase processes are more important for capturing the difference between active and break composites, while convection parameterization is relatively more important for the intraseasonal variance analyses. During active (break) phase of monsoon deeper (weaker) convection (as revealed in the analysis of OLR, Supplementary Fig. 2) helps for the formation of more (less) upper-level cloud condensate. Therefore, ice-phase microphysical processes (i.e., ice deposition, freezing, condensation, riming, etc.) and thermodynamical phase changes are more prominent for capturing the difference between active and break composites. On the other hand, for intraseasonal variance analyses, convection parameterization is relatively more important because it depends on the large-scale supply of moisture (e.g., Ham and Hong 2013). The availability of moisture or specific humidity is determined by the different types of convection schemes. As a result, prominent differences are seen between SAS and NSAS convection scheme for intraseasonal variance analyses.

In a nutshell, to explain the mechanism, we have presented a schematic diagram in Fig. 15. Proper representation of upper-level cloud condensate in ICE run (i.e., with ice phase microphysics) leads to proper representation of specific humidity in active and break spells. Better representation of upper-level cloud condensate further (though latent heating, Hazra et al. 2017a) leads to realistic modulation of atmospheric circulation and better simulation of convection (as represented by OLR) in active and break spell of ICE run. As a result, better simulation of active and break occurs in the ICE run (Fig. 15a).

In contrast, NOICE run (i.e., with warm phase microphysics) has no significant amount of upper-level cloud condensate in the active phase. It leads to an improper representation of specific humidity. Also, there is an insignificant difference of OLR (convection) between active and break simulation in NOICE run. Unrealistic modulation of

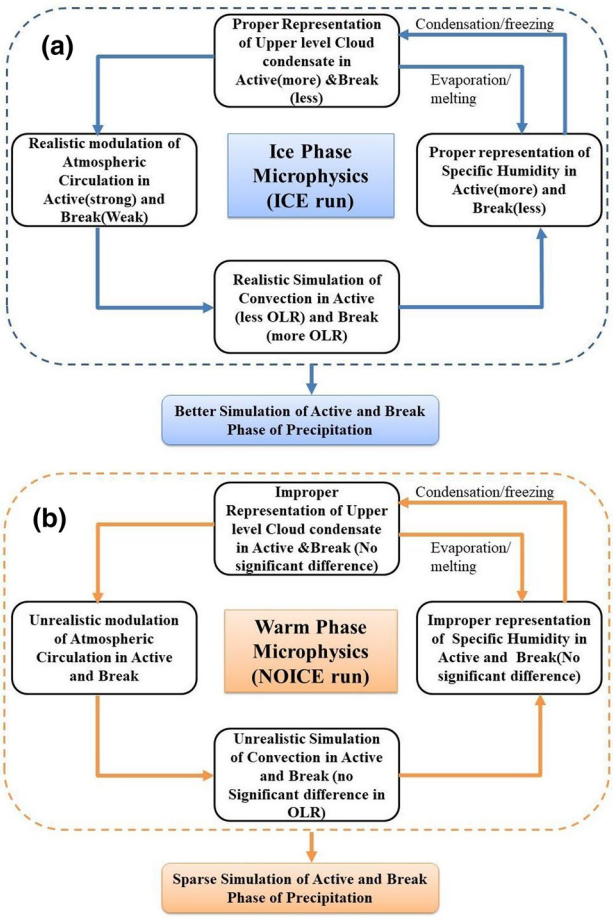

Fig. 15 Schematic diagram illustrating possible mechanism for the betterment of active and break simulation in **a** ice phase microphysics (ICE run) and **b** unrealistic (sparse) simulation of active and break in warm phase microphysics (NOICE run) simulations

atmospheric circulation is noted, and hence convection is suppressed in the active phase. As a result, NOICE runs simulated active, and break phase is scattered/sparse (not simulated realistically) (Fig. 15b).

Thus, the study has highlighted the important role of ice-microphysics and convective parameterization for the improved simulation of ISMR and MISO.

Acknowledgements Authors are thankful to Prof. Ravi S. Nanjundiah, Director, Indian Institute of Tropical Meteorology (IITM), for encouraging to carry out this research work. We are thankful to the anonymous reviewers for the improvement in the manuscript. The model simulation is also archived at 'Aaditya' HPC system at IITM and available upon request from the corresponding author. The authors have no conflicts of interest to declare.

References

Abhik S, Mukhopadhyay P, Goswami BN (2014) Evaluation of mean and intraseasonal variability of Indian summer monsoon simulation in ECHAM5: identification of possible source of bias. Clim Dyn 43:389–406

Abhik S, Krishna RPM, Mahakur M, GanaiM MP, Dudhia J (2017) Revised cloud processes to improve the mean and intraseasonal variability of Indian summer monsoon in climate forecast system: part 1. J Adv Mod Earth Syst 9:1002–1029

Abhilash S, Sahai AK, Pattnaik S, Goswami BN, Kumar A (2014) Extended range prediction of active-break spells of Indian summer monsoon rainfall using an ensemble prediction system in NCEP climate forecast system. Int J Climatol 34:98–113. https://doi.org/10.1002/joc.3668

Abish B, Joseph PV, Johannessen OM (2013) Weakening trend of the tropical easterly jet stream of the Boreal Summer Monsoon Season 1950–2009. J Clim 26:9408–9414. https://doi.org/10.1175/jcli-d-13-00440.1

Adler RF, Huffman GJ, Chang A et al (2003) The version-2 global precipitation climatology project (GPCP) monthly precipitation analysis (1979–Present). J Hydrometeorol 4:1147–1167

Annamalai H, Slingo JM (2001) Active/break cycles: diagnosis of the intraseasonal variability of the Asian Summer Monsoon. Clim Dyn 18:85–102. https://doi.org/10.1007/s003820100161

Anthes RA (1977) A cumulus parameterization scheme utilizing a one-dimensional cloud model. Mon Weather Rev 105:270–286. https://doi.org/10.1175/1520-0493(1977)

Arakawa A, Schubert WH (1974) Interaction of a cumulus cloud ensemble with the large-scale environment, part I. J Atmos Sci 31:674–701

Baisya H, Pattnaik S, Hazra V, Sisodiya A, Rai D (2018) Ramifications of atmospheric humidity on monsoon depressions over the Indian subcontinent. Sci Rep. https://doi.org/10.1038/s41598-018-28365-2

Bergeron T (1935) On the physics of clouds and precipitation. Proces-Verbaux de l'Association de Météorologie. International Union of Geodesy and Geophysics, Brussles, pp 156–178

Betts A, Miller M (1986) A new convective adjustment scheme, Part II: single column tests using GATE wave, BOMEX, ATEX and arctic air-mass data sets. Q J R Meteorol Soc 112:693–709. https://doi.org/10.1256/smsqj.47307

Bombardi RJ, Schneider EK, Marx L, Halder S, Singh B, Tawfik AB, Dirmeyer PA, Kinter JL (2015) Improvements in the representation of the Indian summer monsoon in the NCEP climate forecast system version 2. Clim Dyn 45:2485–2498

Bony S, Stevens B, Jakob DM et al (2015) Clouds, circulation and climate sensitivity. Nat Geosci 8:261–268. https://doi.org/10.1038/ngeo2398

Boyle JS, Klein SA, Lucas DD et al (2015) The parametric sensitivity of CAM5s MJO. J Geophys Res Atmos 120:1424–1444

Cess RD (1989) Gauging water-vapour feedback. Nature 342:736–737

Chakraborty A, Nanjundiah RS (2014) Role of orography in modulating space–time scales of convection over South Asia. Theoret Appl Climatol 116:549–564. https://doi.org/10.1007/s00704-013-0963-4

Chatterjee P, Goswami BN (2004) Structure, genesis and scale selection of the tropical quasi-biweekly mode. Q J R Meteorol Soc 130:1171–1194

Chaudhari HS, Shinde M, Oh J (2010) Understanding of anomalous Indian Summer Monsoon rainfall of 2002 and 1994. Q Int 213:20–32

Chaudhari HS, Pokhrel S, MohantyS SSK (2013) Seasonal prediction of Indian summer monsoon in NCEP coupled and uncoupled model. Theor App Climatol 114:459–477

Chaudhari HS, Hazra A, Saha SK, Dhakate A, Pokhrel S (2016a) Indian summer monsoon simulations with CFSv2: a microphysics perspective. Theor App Climatol 125:253–269

Chaudhari HS, Pokhrel S, Rahman H, Dhakate A, Saha SK, Pentakota S, Gairola RM (2016b) Influence of upper ocean on Indian summer monsoon rainfall: studies by observation and NCEP climate forecast system (CFSv2). Theor App Climatol 125:413–426

Chaudhari HS, Hazra A, Pokhrel S, Saha SK, Talluri SS (2018) Simulation of extreme Indian summer monsoon years in coupled model intercomparison project phase 5 models: role of cloud processes. Int J Climatol 39:901–920. https://doi.org/10.1002/joc.5851

Choudhury AD, Krishnan R (2011) Dynamical response of the South Asian monsoon trough to latent heating from stratiform and convective precipitation. J Atmos Sci 68:1347–1363. https://doi.org/10.1175/2011jas3705.1

Clough S, Shephard M, Mlawer E et al (2005) Atmospheric radiative transfer modeling: a summary of the AER codes. J Quant Spectrosc Radiat Transfer 91:233–244. https://doi.org/10.1016/j.jqsrt.2004.05.058

De S, Hazra A, Chaudhari HS (2016) Does the modification in "critical relative humidity" of NCEP CFSv2 dictate Indian mean summer monsoon forecast? Evaluation through thermodynamical and dynamical aspects. Clim Dyn 46:1197–1222

De S, Agarwal NK, Hazra A, Chaudhari HS, Sahai AK (2019) On unravelling mechanism of interplay between cloud and large scale circulation: a grey area in climate science. Clim Dyn 46:1197–1222

Diao M, Bryan GH, Morrison H, Jensen JB (2017) Ice nucleation parameterization and relative humidity distribution in idealized squall-line simulations. J Atmos Sci 74:2761–2787

Ek MB, Mitchell KE, Lin Y, Rogers E, Grunmann P, Koren V, Gayno G, Tarpley JD (2003) Implementation of Noah land surface model advances in the National Centers for Environmental Prediction operational mesoscale Eta model. J Geophys Res 1089(D22):8851

Ferrier BS, Lin Y, Black T, Rogers E, DiMego G (2002) Implementation of a new grid-scale cloud and precipitation scheme in the NCEP Eta model. In: Preprints, 15th conference on numerical weather prediction, San Antonio, TX, American Meteorological Society, pp 280–283

Field PR, Heymsfield AJ (2015) Importance of snow to global precipitation. Geophy Res Lett 42:9512–9520. https://doi.org/10.1002/2015gl065497

Fu D, Guo X, Liu C (2011) Effects of cloud microphysics on monsoon convective system and its formation environments over

the South China Sea: a two-dimensional cloud-resolving modeling study. J Geophy Res. https://doi.org/10.1029/2010jd014662

Gadgil S (2007) The Indian monsoon. Resonance 12:4–20. https://doi.org/10.1007/s12045-007-0045-y

Ganai M, Mukhopadhyay P, Krishna RPM, Mahakur M (2015) The impact of revised simplified Arakawa-Schubert convection parameterization scheme in CFSv2 on the simulation of the Indian summer monsoon. Clim Dyn 45:881–902. https://doi.org/10.1007/s00382-014-2320-4

Ganai M, Krishna RPM, Mukhopadhyay P, Mahakur M (2016) The impact of revised simplified Arakawa-Schubert scheme on the simulation of mean and diurnal variability associated with active and break phases of Indian summer monsoon using CFSv2. J Geophys Res Atmos 121:9301–9323. https://doi.org/10.1002/2016jd025393

Gettelman A, Collins WD, Fetzer EJ et al (2006) Climatology of upper-tropospheric relative humidity from the atmospheric infrared sounder and implications for climate. J Clim 19:6104–6121. https://doi.org/10.1175/jcli3956.1

Goswami BN (1994) Dynamical predictability of seasonal monsoon rainfall: problems and prospects. Proc Indian Natl Sci Acad 60:101–120

Goswami BN (1998) Interannual variations of Indian summer monsoon in a GCM: external conditions versus internal feedbacks. J Clim 11:501–522

Goswami BN, Krishnamurthy V, Aamalai H (1999) A broad-scale circulation index for the interannual variability of the Indian summer monsoon. Q J R Meteorol Soc 125:611–633

Goswami BB, Mani NJ, Mukhopadhyay P et al (2011) Monsoon intraseasonal oscillations as simulated by the superparameterized community atmosphere model. J Geophys Res Atmos. https://doi.org/10.1029/2011jd015948

Goswami BB, Khouider B, Phani R et al (2017) Implementation and calibration of a stochastic multicloud convective parameterization in the NCEP Climate Forecast System (CFSv2). J Adv Model Earth Syst 9:1721–1739. https://doi.org/10.1002/2017ms001014

Griffies SM, Gnanadesikan A, Dixon KW et al (2005) Formulation of an ocean model for global climate simulations. Ocean Sci 1:45–79. https://doi.org/10.5194/os-1-45-2005

Ham S, Hong S (2013) Sensitivity of simulated intraseasonal oscillation to four convective parameterization schemes in a coupled climate model. Asia Pac J Atmos Sci 49:483–496

Han J, Pan H-L (2011) Revision of convection and vertical diffusion schemes in the NCEP global forecast system. Weather Forecast 26:520–533

Hazra A, Chaudhari HS, Rao SA, Goswami BN, Dhakate A, Pokhrel S, Saha SK (2015) Impact of revised cloud microphysical scheme in CFSv2 on the simulation of the Indian summer monsoon. Int J Climatol 35:4738–4755. https://doi.org/10.1002/joc.4320

Hazra A, Chaudhari HS, Pokhrel S, Saha SK (2016) Indian summer monsoon precipitating clouds: role of microphysical process rates. Clim Dyn 46:2551–2571

Hazra A, Chaudhari HS, Saha SK, Pokhrel S (2017a) Effect of cloud microphysics on Indian summer monsoon precipitating clouds: a coupled climate modeling study. J Geophy Res Atmos 122:3786–3805. https://doi.org/10.1002/2016jd026106

Hazra A, Chaudhari HS, Saha SK, Pokhrel S, Goswami BN (2017b) Progress towards achieving the challenge of indian summer monsoon climate simulation in a coupled ocean-atmosphere model. J Adv Model Earth Syst 9:2268–2290. https://doi.org/10.1002/2017ms000966

Hong S-Y, Dudhia J, Chen S-H (2004) A revised approach to ice microphysical processes for the bulk parameterization of clouds and precipitation. Mon Weather Rev 132:103–120

Hu Y, Winker D, Vaughan M et al (2009) CALIPSO/CALIOP Cloud phase discrimination algorithm. J Atmos Oceanic Technol 26:2293–2309. https://doi.org/10.1175/2009jtecha1280.1

Iacono MJ, Mlawer EJ, Clough SA, Morcrette J-J (2000) Impact of an improved longwave radiation model, RRTM, on the energy budget and thermodynamic properties of the NCAR community climate model, CCM3. J Geophy Res Atmos 105:14873–14890. https://doi.org/10.1029/2000jd900091

Joseph PV, Sijikumar S (2004) Intraseasonal variability of the low-level jet stream of the asian summer monsoon. J Clim 17:1449–1458

Kanamitsu M, Ebisuzaki W, Woollen J et al (2002) NCEP–DOE AMIP-II reanalysis (R-2). Bull Am Meteorol Soc 83:1631–1644. https://doi.org/10.1175/bams-83-11-1631

Kang H-S, Hong S-Y (2008) Sensitivity of the simulated East Asian summer monsoon climatology to four convective parameterization schemes. J Geophys Res. https://doi.org/10.1029/2007jd009692

Kim Y-J, Arakawa A (1995) Improvement of orographic gravity wave parameterization using a mesoscale gravity wave model. J Atmos Sci 52:1875–1902

Krishna RPM, Rao SA, Srivastava A et al (2019) Impact of convective parameterization on the seasonal prediction skill of Indian summer monsoon. Clim Dyn 53:6227–6243. https://doi.org/10.1007/s00382-019-04921-y

Krishna Kumar K, Hoerling M, Rajagopalan B (2005) Advancing dynamical prediction of Indian monsoon rainfall. Geophy Res Lett 32:L08704. https://doi.org/10.1029/2004GL021979

Krishnamurti TN, Bhalme HN (1976) Oscillations of a monsoon system. Part I. Observational aspects. J Atmos Sci 33:1937–1954

Krishnamurti TN, Bedi HS, Subramaniam M (1989) The summer monsoon of 1987. J Clim 2:321–340

Krishnan R, Kumar V, Sugi M, Yoshimura J (2009) Internal feedbacks from monsoon-midlatitude interactions during droughts in the Indian Summer Monsoon. J Atmos Sci 66:553–578. https://doi.org/10.1175/2008jas2723.1

Kruegera SK, Fua Q, Lioua KN, Chin HN (1995) Improvements of an ice-phase microphysics parameterization for use in numerical simulations of tropical convection. J Appl Meteorol 34:281–287. https://doi.org/10.1175/1520-0450-34.1.281

Kulkarni A, Kripalani RH (1998) Rainfall patterns over India: classification with fuzzy c-means method. Theor Appl Climatol 59:137–146. https://doi.org/10.1007/s007040050019

Kumar S, Hazra A, Goswami BN (2014) Role of interaction between dynamics, thermodynamics and cloud microphysics on summer monsoon precipitating clouds over the Myanmar Coast and the Western Ghats. Clim Dyn 43:911–924. https://doi.org/10.1007/s00382-013-1909-3

Kumar S, Arora A, Chattopadhyay R, Hazra A, Rao SA, Goswami BN (2017) Seminal role of stratiform clouds in large-scale aggregation of tropical rain in boreal summer monsoon intraseasonal oscillations. Clim Dyn 48:999–1015. https://doi.org/10.1007/s00382-016-3124-5

Li J, Wu K, Li F et al (2017) Effects of latent heat in various cloud microphysics processes on autumn rainstorms with different intensities on Hainan Island, China. Atmos Res 189:47–60

Liebemann B, Smith AC (1996) Description of a complete (interpolated) outgoing longwave radiation dataset. Bull Am Meteorol Soc 77:1275–1277

Liu X, Xie S, Ghan SJ (2007) Evaluation of a new mixed-phase cloud microphysics parameterization with CAM3 single-column model and M-PACE observations. Geophy Res Lett 34:L23712

Liu D, Yang B, Zhang Y et al (2018) Combined impacts of convection and microphysics parameterizations on the simulations of precipitation and cloud properties over Asia. Atmos Res 212:172–185

Lord SJ (1982) Interaction of a cumulus cloud ensemble with large-scale environment. Part III: semi-prognostic test of the

Arakawa–Schubert cumulus parameterization. J Atmos Sci 39:88–103
Lott F, Miller MJ (1997) A new subgrid-scale orographic drag parameterization: its formulation and testing. Q J R Meteorol Soc 123:101–127. https://doi.org/10.1256/smsqj.53703
Lund IA (1963) Map-pattern classification by statistical methods. J Appl Meteorol 2:56–65
Mandke SK, Sahai AK, Shinde MA, Joseph S, Chattopadhyay R (2007) Simulated changes in active/break spells during the Indian summer monsoon due to enhanced CO_2 concentrations: assessment from selected coupled atmosphere–ocean global climate models. Int J Climatol 27:837–859. https://doi.org/10.1002/joc.1440
Mccumber M, Tao W-K, Simpson J, Pencb R, Soong ST (1991) Comparison of ice-phase microphysical parameterization schemes using numerical simulations of tropical convection. J Appl Meteorol 30:985–1004. https://doi.org/10.1175/1520-0450-30.7.985
Mlawer EJ, Taubman SJ, Brown PD, IaconoMJ CSA (1997) Radiative transfer for inhomogeneous atmospheres: RRTM, a validated correlated-k model for the longwave. J Geophy Res Atmos 102:16663–16682. https://doi.org/10.1029/97jd00237
Mukhopadhyay P, Taraphdar S, Goswami BN, Krishnakumar K (2010) Indian summer monsoon precipitation climatology in a high-resolution regional climate model: impacts of convective parameterization on systematic biases. Weather Forecast 25:369–387. https://doi.org/10.1175/2009waf2222320.1
Murakami T (1976) Analysis of summer monsoon fluctuations over India. J Meteorol Soc Jpn 54:15–31. https://doi.org/10.2151/jmsj1965.54.1_15
Murakami T (1980) Temporal variations of satellite-observed outgoing longwave radiation over the winter monsoon region. Part II: short-period (4–6 day) oscillations. Mon Weather Rev 108:427–444
Naidu C, Krishna KM, Rao SR, Bhanu Kumar OSRU, Durgalakshmi K, Ramakrishna SSVS (2011) Variations of Indian summer monsoon rainfall induce the weakening of easterly jet stream in the warming environment? Global Planet Change 75:21–30. https://doi.org/10.1016/j.gloplacha.2010.10.001
Nithya K, Manoj MG, Mohankumar K (2017) Effect of El Niño/La Niña on tropical easterly jet stream during Asian summer monsoon season. Int J Climatol 37:4994–5004. https://doi.org/10.1002/joc.5137
Noda AT, Satoh M, Yamada Y, Kodama C, Miyakawa T, Seiki T (2015) Cold and warm rain simulated using a global nonhydrostatic model without cumulus parameterization and their responses to global warming. J Meteorol Soc Jpn 93:181–197
Parthasarathy B, Munot A, Kothawale D (1988) Regression model for estimation of Indian food grain production from summer monsoon rainfall. Agric For Meteorol 42:167–182
Pattnaik S, Abhilash S, De S et al (2013) Influence of convective parameterization on the systematic errors of climate forecast system (CFS) model over the Indian monsoon region from an extended range forecast perspective. Clim Dyn 41:341–365. https://doi.org/10.1007/s00382-013-1662-7
Prasad KD, Verma RK (1985) Large-scale features of satellite-derived outgoing long-wave radiation in relation to monsoon circulation over the Indian region. Int J Climatol 5:297–306. https://doi.org/10.1002/joc.3370050306
Quaas J (2012) Evaluating the "critical relative humidity" as a measure of subgrid-scale variability of humidity in general circulation model cloud cover parameterizations using satellite data. J Geophys Res Atmos 117:D09208. https://doi.org/10.1029/2012JD017495
Rahman SH, Simon B (2006) Summer monsoon intraseasonal oscillation over eastern Arabian sea—as revealed by TRMM microwave imager products. J Earth Syst Sci 115:575–586. https://doi.org/10.1007/bf02702910
Rajeevan M, Gadgil S, Bhate J (2010) Active and break spells of the Indian summer monsoon. J Earth Syst Sci 119:229–247. https://doi.org/10.1007/s12040-010-0019-4
Rajeevan M, Unnikrishnan CK, Preethi B (2012) Evaluation of the ENSEMBLES multi-model seasonal forecasts of Indian summer monsoon variability. Clim Dyn 38:2257–2274
Raju PVS, Mohanty UC, Bhatla R (2005) Onset characteristics of the southwest monsoon over India. Int J Climatol 25:167–182. https://doi.org/10.1002/joc.1121
RieneckerMM SMJ, Gelaro R et al (2011) MERRA: NASA's modern-era retrospective analysis for research and applications. J Clim 24:3624–3648
Rossow WB, Schiffer RA (1999) Advances in understanding clouds from ISCCP. Bull Am Meteorol Soc 80:2261–2287
Saha SK, Pokhrel S, Chaudhari HS (2013) Influence of Eurasian snow on Indian summer monsoon in NCEP CFSv2 freerun. Clim Dyn 41:1801–1815. https://doi.org/10.1007/s00382-012-1617-4
Saha S, Moorthi S, Wu X et al (2014a) The NCEP climate forecast system version 2. J Clim 27:2185–2208. https://doi.org/10.1175/JCLI-D-12-00823.1
Saha SB, Roy SS, Bhowmik SKR, Kundu PK (2014b) Intra-seasonal variability of cloud amount over the Indian subcontinent during the monsoon season as observed by TRMM precipitation radar. Geofizika. https://doi.org/10.15233/gfz.2014.31.2
Saha SK, Pokhrel S, Chaudhari HS, Dhakate A, Shewale S, Sabeerali CT, Salunke S, Hazra A, Mohapatra S, Rao SA (2014c) Improved simulation of Indian summer monsoon in latest NCEP climate forecast system free run. Int J Climatol 34:1628–1641. https://doi.org/10.1002/joc.3791
Saha SK, Hazra A, Pokhrel S, Chaudhari HS, Sujith K, Rai A, Rahaman H, Goswami BN (2019) Unraveling the mystery of indian summer monsoon prediction: improved estimate of predictability limit. J Geophys Res Atmos. https://doi.org/10.1029/2018jd030082
Sikka DR, Gadgil S (1980) On maximum cloud zone and ITCZ over Indian longitude during the southwest monsoon. Mon Weather Rev 108:1840–1853
Song X, Zhang GJ (2011) Microphysics parameterization for convective clouds in a global climate model: description and single-column model tests. J Geophys Res. https://doi.org/10.1029/2010jd014833
Straka JM, Anderson JR (1993) Numerical simulations of microburst-producing storms: some results from storms observed during COHMEX. J Atmos Sci 50:1329–1348. https://doi.org/10.1175/1520-0469(1993)050
Sud YC, Walker GK (1999) Microphysics of clouds with the relaxed Arakawa-Schubert scheme (McRAS). Part I: design and evaluation with GATE phase III data. J Atmos Sci 56:3196–3220. https://doi.org/10.1175/1520-0469(1999)056
Sundqvist H (1988) Parameterization of condensation and associated clouds in models for weather prediction and general circulation simulation. In: Schlesinger ME (ed) Physically-based modelling and simulation of climate and climatic change-part-I. Kluwer Academic Publishers, Berlin, pp 433–461. https://doi.org/10.1007/978-94-009-3041-4_10
Sundqvist H, Berge E, Kristjansson JE (1989) Condensation and cloud studies with mesoscale numerical weather prediction model. Mon Weather Rev 117:1641–1757
Tang X, Chen B (2006) Cloud types associated with the Asian summer monsoons as determined from MODIS/TERRA measurements and a comparison with surface observations. Geophy Res Lett 33:L07814. https://doi.org/10.1029/2006GL026004
Tao W-K, Moncrieff MW (2009) Multiscale cloud system modeling. Rev Geophys 47:RG4002
Tao W-K, Simpson J (1989) Modeling study of a tropical squall-type convective line. J Atmos Sci 46:177–202

Thompson A, Stefanova L, Krishnamurti TN (2008) Baroclinic splitting of jets. Meteorol Atmos Phys 100:257–274

Turner AG, Slingo JM (2008) Subseasonal extremes of precipitation and active-break cycles of the Indian summer monsoon in a climate-change scenario. Q J R Meteorol Soc 135:549–567. https://doi.org/10.1002/qj.401

Udelhofen PM, Hartmann DL (1995) Influence of tropical cloud systems on the relative humidity in the upper troposphere. J Geophy Res 100:7423–7440. https://doi.org/10.1029/94jd02826

Umakanth U, Kesarkar AP, Raju A, Rao SVB (2015) Representation of monsoon intraseasonal oscillations in regional climate model: sensitivity to convective physics. Clim Dyn 47:895–917. https://doi.org/10.1007/s00382-015-2878-5

Viswanadhapalli Y, Dasari HP, Dwivedi S et al (2019) Variability of monsoon low-level jet and associated rainfall over India. Int J Climatol 40:1067–1089. https://doi.org/10.1002/joc.6256

Wang B (2005) Fundamental challenge in simulation and prediction of summer monsoon rainfall. Geophy Res Lett. https://doi.org/10.1029/2005gl022734

Wang P-H, Minnis P, Mccormick MP, Kent GS, Skeens KM (1996) A 6-year climatology of cloud occurrence frequency from stratospheric aerosol and gas experiment II observations (1985–1990). J Geophy Res Atmos 101:29407–29429. https://doi.org/10.1029/96jd01780

Wang PK, Lin H-M, Su S-H (2010) The impact of ice microphysical processes on the life span of a mid latitude super cell storm. Atmos Res 97:450–461. https://doi.org/10.1016/j.atmosres.2010.05.006

Webster PJ, Magaña VO, Palmer TN et al (1998) Monsoons: processes, predictability, and the prospects for prediction. J Geophy Res Oceans 103:14451–14510. https://doi.org/10.1029/97jc02719

Wheeler M, Kiladis GN (1999) Convectively coupled equatorial waves: analysis of clouds and temperature in the wavenumber-frequency domain. J Atmos Sci 56:374–399. https://doi.org/10.1175/1520-0469(1999)056

Wilson SS, Joseph PV, Mohanakumar K, Johannessen OM (2018) Interannual and long term variability of low level jetstream of the Asian summer monsoon. Tellus A Dyn Meteorol Oceanogr 70:1–9. https://doi.org/10.1080/16000870.2018.1445380

Wylie D, Menzel W (1999) Eight years of high cloud statistics using HIRS. J Clim 12:170–184

Yang B, Zhang Y, Qian Y et al (2015) Parametric sensitivity analysis for the Asian summer monsoon precipitation simulation in the Beijing Climate Center AGCM, version 2.1. J Clim 28:5622–5644. https://doi.org/10.1175/jcli-d-14-00655.1

Yasunari T (1980) A quasi-stationary appearance of 30 to 40 day period in the cloudiness fluctuations during the summer monsoon over India. J Meteorol Soc Jpn Ser II 58:225–229. https://doi.org/10.2151/jmsj1965.58.3_225

Zhang D-L (1989) The effect of parameterized ice microphysics on the simulation of vortex circulation with a mesoscale hydrostatic model. Tellus A 41A:132–147. https://doi.org/10.1111/j.1600-0870.1989.tb00371.x

Zhang GJ, Song X (2016) Parameterization of microphysical processes in convective clouds in global climate models. Meteorol Monogr 56:12.1–12.18. https://doi.org/10.1175/amsmonographs-d-15-0015.1

Zhao Q, Carr FH (1997) A prognostic cloud scheme for operational NWP models. Mon Weather Rev 125:1931–1953